3rd Workshop on Maritime Computer Vision (MaCVi) 2025: Challenge Results

Benjamin Kiefer[0,1], Lojze Žust[2], Jon Muhovič[2], Matej Kristan[2], Janez Perš[2], Matija Teršek[3],
Uma Mudenagudi[6], Chaitra Desai[6], Arnold Wiliem[4,5], Marten Kreis[1], Nikhil Akalwadi[6],
Yitong Quan[1], Zhiqiang Zhong[7], Zhe Zhang[7], Sujie Liu[7], Xuran Chen[7], Yang Yang[7],
Matej Fabijanić[8], Fausto Ferreira[8], Seongju Lee[9], Junseok Lee[9], Kyoobin Lee[9],
Shanliang Yao[17], Runwei Guan[11], Xiaoyu Huang[10], Yi Ni[12], Himanshu Kumar[13], Yuan Feng[14],
Yi-Ching Cheng[15], Tzu-Yu Lin[15], Chia-Ming Lee[15], Chih-Chung Hsu[15], Jannik Sheikh[16],
Andreas Michel[16], Wolfgang Gross[16], Martin Weinmann[21], Josip Šarić[2], Yipeng Lin[7], Xiang Yang[7],
Nan Jiang[18], Yutang Lu[19], Fei Feng[19], Ali Awad[20], Evan Lucas[20], Ashraf Saleem[20],
Ching-Heng Cheng[15], Yu-Fan Lin[15], Tzu-Yu Lin[15], Chih-Chung Hsu[15]

[0]LOOKOUT, [1]University of Tuebingen, [2]University of Ljubljana, [3]Luxonis, [4]Shield AI,
[5]Queensland University of Technology, [6]Center of Excellence in Visual Intelligence,
KLE Technological University, [7]Nanjing University of Science and Technology,
[8]University of Zagreb Faculty of Electrical Engineering and Computing, [9]Gwangju Institute
of Science and Technology (GIST), [10]University of Liverpool, [11]Hong Kong
University of Science and Technology (Guangzhou), [12]Xi'an Jiaotong-Liverpool University,
[13]Independent Researcher, [14]Dalian Maritime University, School of Marine Engineering,
[15]National Cheng Kung University, [16]Fraunhofer IOSB, [17]Yancheng Institute of Technology,
[18]Nanjing University, [19]Beijing University of Posts and Telecommunications,
[20]Michigan Technological University [21]Karlsruhe Institute of Technology

Abstract

The 3rd Workshop on Maritime Computer Vision (MaCVi) 2025 addresses maritime computer vision for Unmanned Surface Vehicles (USV) and underwater.

This report offers a comprehensive overview of the findings from the challenges. We provide both statistical and qualitative analyses, evaluating trends from over 700 submissions. All datasets, evaluation code, and the leaderboard are available to the public at `https://macvi.org/workshop/macvi25`.

1. Introduction

Maritime environments, with their unique challenges such as dynamic lighting, reflections, and cluttered scenes, demand specialized computer vision techniques [24, 31, 33, 54, 65]. Autonomous systems like Unmanned Surface Vehicles (USVs) and Underwater Vehicles (UUVs) rely heavily on robust vision algorithms to navigate, detect, and interpret complex surroundings [5, 34, 84]. Addressing these challenges requires not only cutting-edge algorithms but
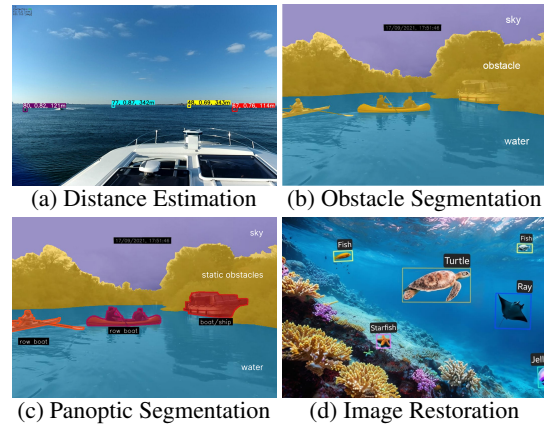

Figure 1: Overview of MaCVi2025 challenges. Challenges include USV-based (a) Distance Estimation, (b) Regular and Embedded Obstacle Segmentation, (c) Panoptic Segmentation, and UUV-based (d) Image Restoration.

also standardized benchmarks and a collaborative research ecosystem [4, 6, 18, 38].

The 3rd Workshop on Maritime Computer Vision (MaCVi 2025) builds on the momentum of the previous two iterations [32, 35] to foster innovation in maritime computer vision. This year, the workshop presented a suite of challenges, including distance estimation, (embedded) semantic & panoptic segmentation, and image restoration. These tasks reflect advancements in dataset availability and evaluation protocols while emphasizing real-world deployment, including embedded hardware.

This report highlights the methodologies, results, and insights from the MaCVi 2025 challenges. The rest of the paper is structured as follows: Section 2 details the general challenge protocols while Sections 3 and 4 discuss the outcomes of individual tracks. All datasets, evaluation tools, and leaderboards are available at `https://macvi.org/workshop/macvi25`.

2. Challenge Participation Protocol

As for the first two challenge iterations, all challenges followed a superset of rules and protocols outlined in this section while challenge specific rules are described in the respective subsections.

2.1. Submission Process

Participants could get the challenge rules and resources on the workshop webpages. There, we provided links to evaluation code, datasets and starter kits.

Then, participants submitted their models and predictions through the official evaluation server. General submission requirements included:

- Predictions formatted according to standardized task-specific formats.

- Compliance with model submission guidelines, including export to ONNX format where applicable.

- A limit of 1-3 submission per day per challenge track.

2.2. Evaluation Server and Leaderboard

An online evaluation server provided automated scoring for all submissions. Test set evaluations were conducted on the server, with results displayed on public leaderboards. The leaderboards were frozen (results of each method visible only to its authors) a week prior to the results announcement to encourage competition and submissions without relying on the results from other teams.

2.3. Timeline

The timeline for all MaCVi 2025 challenges was:

- **Submissions open:** 13th Sep 2024

- **Leaderboards frozen:** 12th Dec 2024

- **Submissions closed:** 19th Dec 2024

2.4. Recognition and Rewards

After additional manual review of the submissions, the top team(s) in each challenge were determined by the challenge-specific metrics and whether the performance was above the provided baselines. They then were invited to submit a short technical report detailing their methods. These reports will are included in the appendix below. Winners were also acknowledged during the workshop and featured on the official website. Additionally, there were prizes for some of the competitions as described on the workshop website.

3. USV-based Perception Challenges

3.1. Approximate Supervised Distance Estimation

Distance estimation using monocular vision is a complex problem that has gained considerable attention in recent years due to its key role in fields such as autonomous driving and robotics [51]. This approach is equally crucial for maritime applications, where it can support essential tasks such as navigation and path planning for unmanned surface vehicles (USVs). State-of-the-art monocular depth estimation frameworks, such as MiDAS [57] and SPI-Depth [39], show significant limitations for this type of application, particularly in terms of real-time performance and accuracy for smaller, distant objects. In addition, many of these approaches generate depth maps with values normalized between 0 and 1, rather than providing the metric distances required for practical use.

In the context of this challenge, participants are required to develop novel methods for estimating distances to maritime navigational aids while simultaneously detecting them in images. To facilitate this, we provide a dataset comprising approximately 3,000 labeled training samples, including single-class normalized bounding-box coordinates and the metric distance between the camera and the object. The ground truth distance is calculated using the Haversine formula, which computes the distance between the GNSS coordinates of the ship, where the camera is mounted, and the corresponding navigational buoys as mapped on a nautical chart. Additionally, participants are provided with a modified version of the YOLOv7 object detector [67], similar to an approach developed by Vajgl *et al.* [64], where the predicted tensor for each anchor consisting of $[c_x, c_y, w, h, p_{obj}, p_{class\_1}, ..., p_{class\_n}]$ is extended by a distance estimate.

The complete dataset includes 2,940 annotated images in the training split and 2,268 in the test split. A detailed distribution of individual objects in both splits, categorized by ground truth distance, is depicted in Figure 2. We chose to include challenging scenarios where buoys are distant and barely visible, aiming to assess the limits of the object detec-
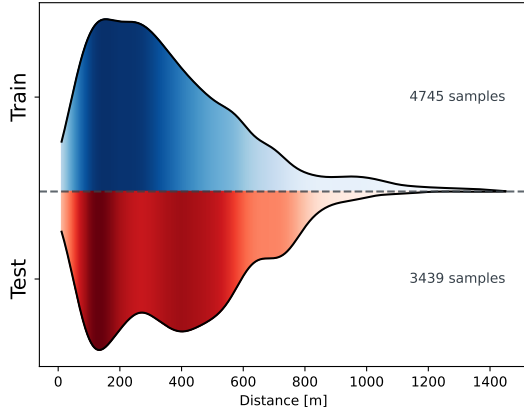
Figure 2: Distribution of samples in the training (■) and test (■) splits with respect to the ground truth distance

Figure 3: Common buoy types in the supervised distance estimation dataset

tion models. Maritime navigational aids exhibit significant variation in size and appearance. Figure 3 highlights the most common buoy types, predominantly comprising red and green channel markers.

3.1.1 Evaluation Protocol

To evaluate the methods submitted by participants, we utilize metrics that assess both object detection performance and distance estimation accuracy. For object detection performance, we employ well-established metrics, specifically AP_{50} and $AP_{50:95}$. The AP_{50} metric calculates the average precision across varying confidence thresholds with an IoU threshold of 50%. In contrast, $AP_{50:95}$ averages the precision over a range of IoU thresholds from 50% to 95% in increments of 5%.

To evaluate the deviation of distance estimates from ground truth values, we define the *absolute error* (ϵ_{abs}) and *relative error* (ϵ_{rel}) as follows:

$$\epsilon_{abs} = \frac{1}{n} \sum_{i=1}^{n} \left| \hat{d}_i - d_i \right|,$$

$$\epsilon_{rel} = \frac{1}{n} \sum_{i=1}^{n} \frac{c_i}{\sum_{j=1}^{n} c_j} \left| \frac{\hat{d}_i - d_i}{d_i} \right|,$$

where n is the total number of predictions, $\hat{d}_i$ denotes the predicted distance, d_i represents the ground truth distance and c_i is the predicted confidence. It is important to note that each distance prediction is weighted by the corresponding normalized confidence for ϵ_{rel}. Furthermore, we include the relative distance error to penalize deviations between the prediction and ground truth more heavily for objects that are in closer proximity.

Finally, the combined quality measure Q is defined as

$$Q = AP_{50:95} \cdot (1 - \min(\epsilon_{rel}, 1)),$$

incorporating both object detection and distance estimation performance.

The submitted models must comply with the following guidelines for performance considerations.

- Model size should not exceed 50 million parameters
- Models have to be exported to *ONNX* format
- The onnx export should not include *NMS*
- Images of testset are rescaled to *1024x1024*

3.1.2 Submissions, Analysis and Trends

60 Submission from 6 different teams, including one baseline model from the MaCVi2025 committee [34], were evaluated. Table 1 displays the results of the challenge. Both top submissions outperform the baseline model in object detection performance and distance estimation metrics. However, the winning model is significantly better with regards to the object detection (AP) metrics, while the second-place submission excels in minimizing the distance estimation errors. In the following section the top two submissions are compared to the provided baseline model. Figure 5 illustrates the distance estimation capabilities of the submitted models. The best-performing model for this task is *Yolov7 Depth-Widened*, however both approaches are capable of significantly reducing the absolute error compared to the baseline, particularly for objects in closer proximity. This is mainly achieved by limiting the number of large outlier

Table 1: Comparison of the performance of the submitted methods and the organizer-provided baseline model (highlighted in gray) on the test split. Performance metrics include object detection measures: AP_{50}, AP_{50-95}, and distance estimation metrics: relative error (ϵ_{rel}) and absolute error (ϵ_{abs}). The overall quality score (**Q**) evaluates both object detection and distance estimation capabilities.

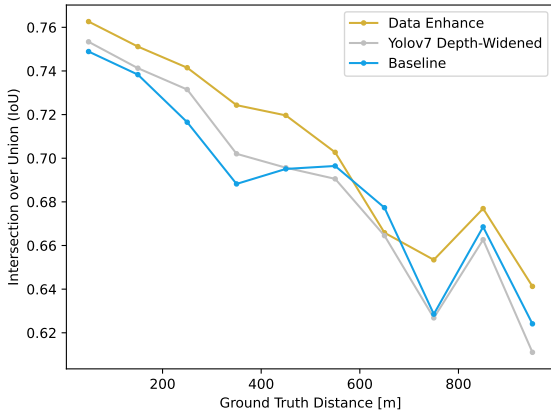| Place	Method	Institution	**Q**↓	AP_{50}	AP_{50-95}	ϵ_{rel}	ϵ_{abs}
①	Data Enhance	NJUST-KMG	**0.2719**	**0.742**	**0.320**	0.149	54.450
②	Yolov7 Depth Widened	UNIZG FER	0.2554	0.729	0.299	**0.145**	**51.170**
-	Baseline	MaCVi	0.2260	0.676	0.274	0.175	59.608

Figure 4: Mean IoU over the distance to the objects with a step size of 100 meters for the top 2 submissions compared with the baseline model

estimates and can likely be attributed to the design of the challenge metric, which penalizes incorrect estimates for nearby objects more severely than for distant objects. Figure 4 shows the mean IoU for increasing distances to the detected objects. As can be seen, the model that received the first place almost always scores highest among its competitors throughout the entire interval.

Both approaches are based on a modified YOLOv7 architecture capable of predicting distance estimates. The *Data Enhance* method (Section A.1) extends this model with an additional object detection head, designed specifically for identifying small objects within the image. This enhancement includes the introduction of a small anchor box, tailored for detecting small, distant buoys composed of only a few pixels. Additionally, a BiFormer [44] is incorporated into the architecture, enabling the model to attend to both local and global feature representations, thereby enhancing object detection performance. This improvement is particularly evident in the model's increased sensitivity to smaller objects, enabled by the attention mechanism. Furthermore, SimAM [74], a parameter-free attention mechanism that identifies and prior-

itizes critical neurons, is integrated into the network to boost object detection performance without increasing model complexity. A diverse range of data augmentation techniques, including translation, rotation, flipping, scaling, and mosaic, are applied to the dataset. Among these, data augmentation and the integration of the additional detection head have the most significant impact on improving the combined quality measure.

The second-place approach *YOLOv7 Depth-Widened* (Section A.2) modifies the model architecture by increasing the number of feature channels of each layer, thereby extending the total parameter count to 49 million parameters. Furthermore, the distance loss function is adapted by doubling the loss for objects that are closer than 441 meters, to improve the relative distance error, where nearby objects are penalized more strictly. As with the winning approach a variety of augmentation techniques are employed, specifically horizontal flipping, HSV-augmentation and using a scale parameter to shrink or enlarge the training images. The technique that leads to the most significant improvement of the quality measure for the second place submission is to use data augmentation, in particular setting the scale parameter to improve the performance for distant, barely visible channel markers.

3.1.3 Discussion and Challenge Winners

The winners of the USV Supervised Object Distance Estimation challenge are:

1st place: Nanjing University of Science and Technology with *Data Enhance*

2nd place: FER LABUST with *YOLOv7 Depth-Widened*

The analysis demonstrates that both methods significantly outperform the baseline model in terms of object detection and distance estimation. Although most architectural modifications were primarily aimed at enhancing object detection performance, the results indicate that these adaptations can also contribute to improvements in distance estimation accuracy.
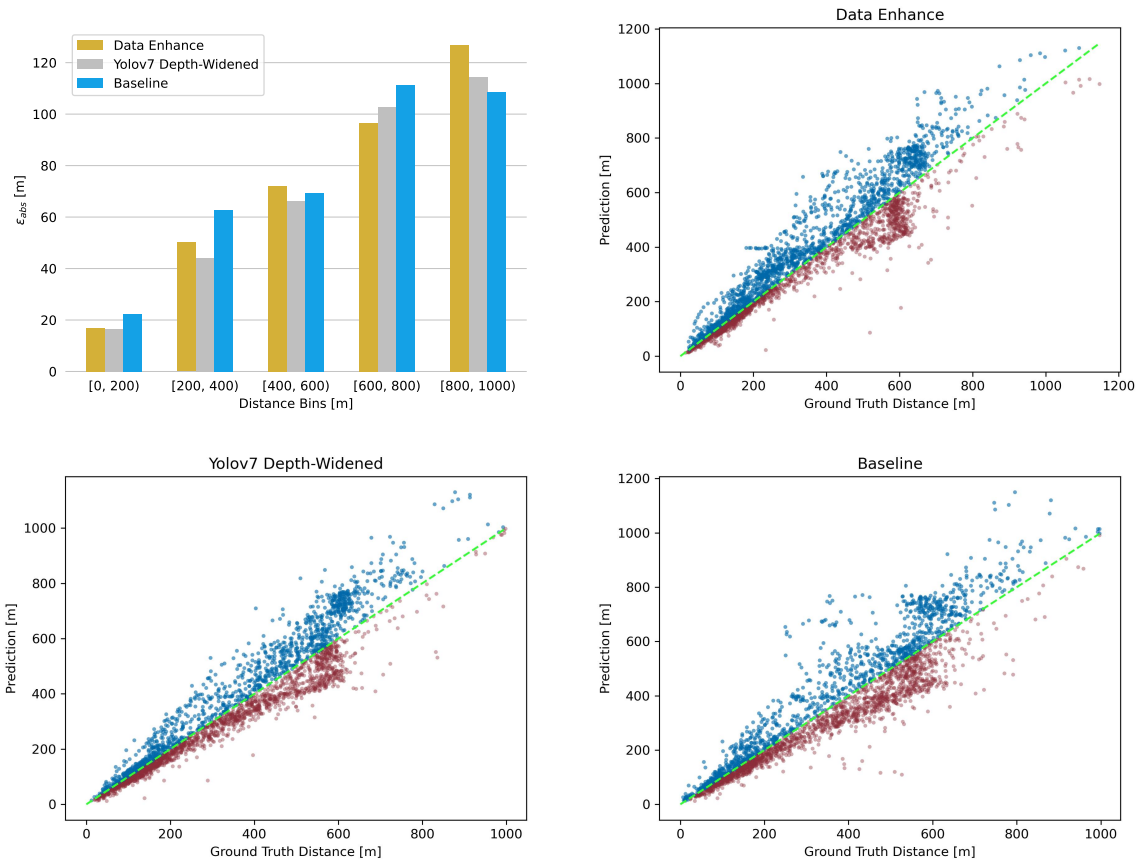
Figure 5: Distance Estimation Results comparing the top two submissions, *Data Enhance* and *Yolov7 Depth Widened*, against the provided baseline model with the absolute error metric (ϵ_{abs}).

3.2. USV-based Obstacle Segmentation Challenge

The methods participating in the USV-based Obstacle Segmentation Challenge were required to predict the scene segmentation (into obstacles, water and sky) for a given input image. The submitted methods have been evaluated on the recently released LaRS benchmark [86]. In addition to the publicly available training set, the authors were also allowed to use additional datasets (upon declaration) for training their methods.

3.2.1 Evaluation Protocol

To evaluate segmentation predictions, we employ the LaRS [86] semantic segmentation evaluation protocol. Segmentation methods provide per-pixel labels of semantic components (water, sky and obstacles). However, traditional approaches for segmentation evaluation (*e.g.* mIoU) do not consider the aspects of predictions that are relevant for USV navigation. Instead, the LaRS protocol evaluates the predicted segmentations with respect to the downstream tasks

of navigation and obstacle avoidance and focuses on the detection of obstacles.

The detection of static obstacles (*e.g.* shoreline) is measured by the water-edge accuracy (μ), which evaluates the segmentation accuracy around the boundary between the water and static obstacles. On the other hand, the detection of dynamic obstacles (*e.g.* boats, buoys, swimmers) is evaluated by counting true-positive (TP), false-positive (FP) and false-negative (FN) detections, summarized by the F1 score. A ground-truth obstacle is counted as a TP if the intersection with the predicted obstacle segmentation is sufficient, otherwise it is counted as a FN. FPs are counted as the number of segmentation blobs (after connected components) on areas annotated as water in ground truth. For further details, please see [86].

The detection F1 score is a great indicator of the quality of the method predictions, as all obstacles have equal importance in the final score, regardless of their size. However, in the trivial case of predicting everything as an obstacle, all ground-truth obstacles will be counted as TP and there will be only one FP blob per image (albeit very large), which

Table 2: Performance of the top three submitted segmentation methods and last year's top three best performing methods (denoted in gray) on the LaRS test set. Performance is reported in terms of water-edge accuracy (μ), precision (Pr), recall (Re), F1 score, segmentation mIoU, and overall quality (Q = mIoU × F1).

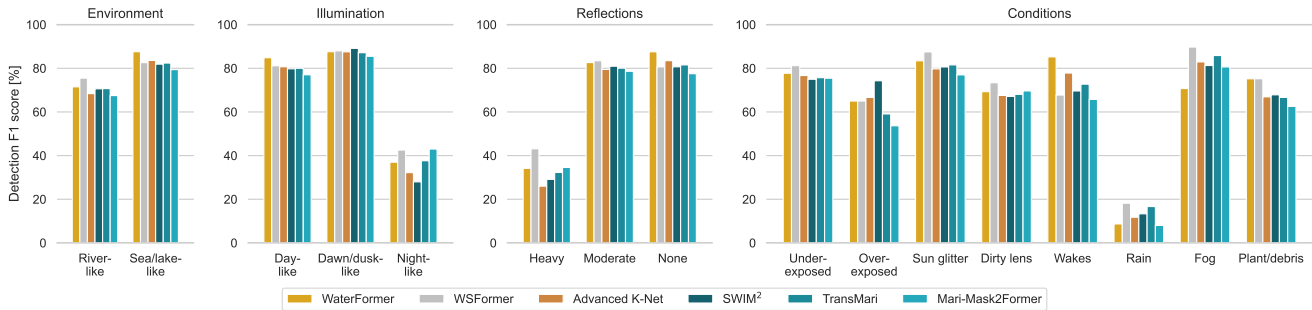| place	method	architecture	Q↓	μ	Pr	Re	F1	mIoU
1	WaterFormer [§B.1]	Mask2Former	**83.2**	80.5	81.6	**88.0**	**84.7**	**98.3**
2	WSFormer [§B.2]	Mask2Former	79.8	**80.6**	**82.9**	79.8	81.3	98.1
3	Advanced K-Net [§B.3]	K-Net	79.0	79.7	77.6	84.2	80.8	97.8
1	SWIM	Mask2Former	78.1	79.7	76.9	83.0	79.9	97.8
2	TransMari	Mask2Former	77.8	79.6	78.5	82.0	80.2	97.1
3	Mari-Mask2Former	Mask2Former	75.7	78.4	79.7	75.1	77.3	97.8

Figure 6: Performance of top segmentation methods with respect to different scene attributes.
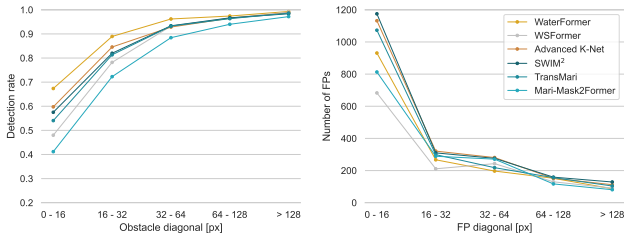

Figure 7: Obstacle detection rate and number of FPs across different sizes of obstacles for top performing methods.

leads to a very large F1 score. On the other hand, mIoU measures the overall segmentation quality on a per-pixel level, but does not reflect the detection of smaller obstacles very well. We thus combine the two measures into a single quality measure (Q = F1 · mIoU) and use it as the primary performance measure in this challenge.

3.2.2 Submissions, Analysis and Trends

The USV-based obstacle segmentation challenge received 59 submissions from 16 teams. Only the best performing method from each team is included in the final challenge results. The results of the submitted methods are available on the public leaderboards of the challenge on the MaCVi web-site [36]. Table 2 presents the top three performing methods participating in the challenge, along with the top three performing methods from the previous MaCVi challenge. This section will focus on analyzing the three best-performing submissions, which were the only ones that improved the results of the top performing approach from the previous MaCVi challenge. We refer to teams and their methods by their overall ranking in Table 2 with the notation (#n), where n is the place of the approach. Short descriptions of the top three methods are available in the Appendix B.

This year, three teams improved over the previous year's best performing method, with methods (#1) WaterFormer, (#2) WSFormer, and (#3) Advanced K-Net. The top performing method improved the performance over the last year's winner by 5.1% Q. Of all the methods in Table 2, all but one are based on Mask2Former architecture [13], the exception being Advanced K-Net. WaterFormer included an extra adapter between the layers of DINOv2 backbone layers, and only used LaRS data for training. Additionally, the authors trained the model to predict 4 classes instead of 3 (the obstacle class was split into static and dynamic obstacles, as per the panoptic segmentation labels). The predictions were merged for the evaluation, which was likely the cause of its high performance. The second-best performing method WSFormer also employed Mask2Former architecture, but used the SWIN-L bakcbone. The method was primarily trained
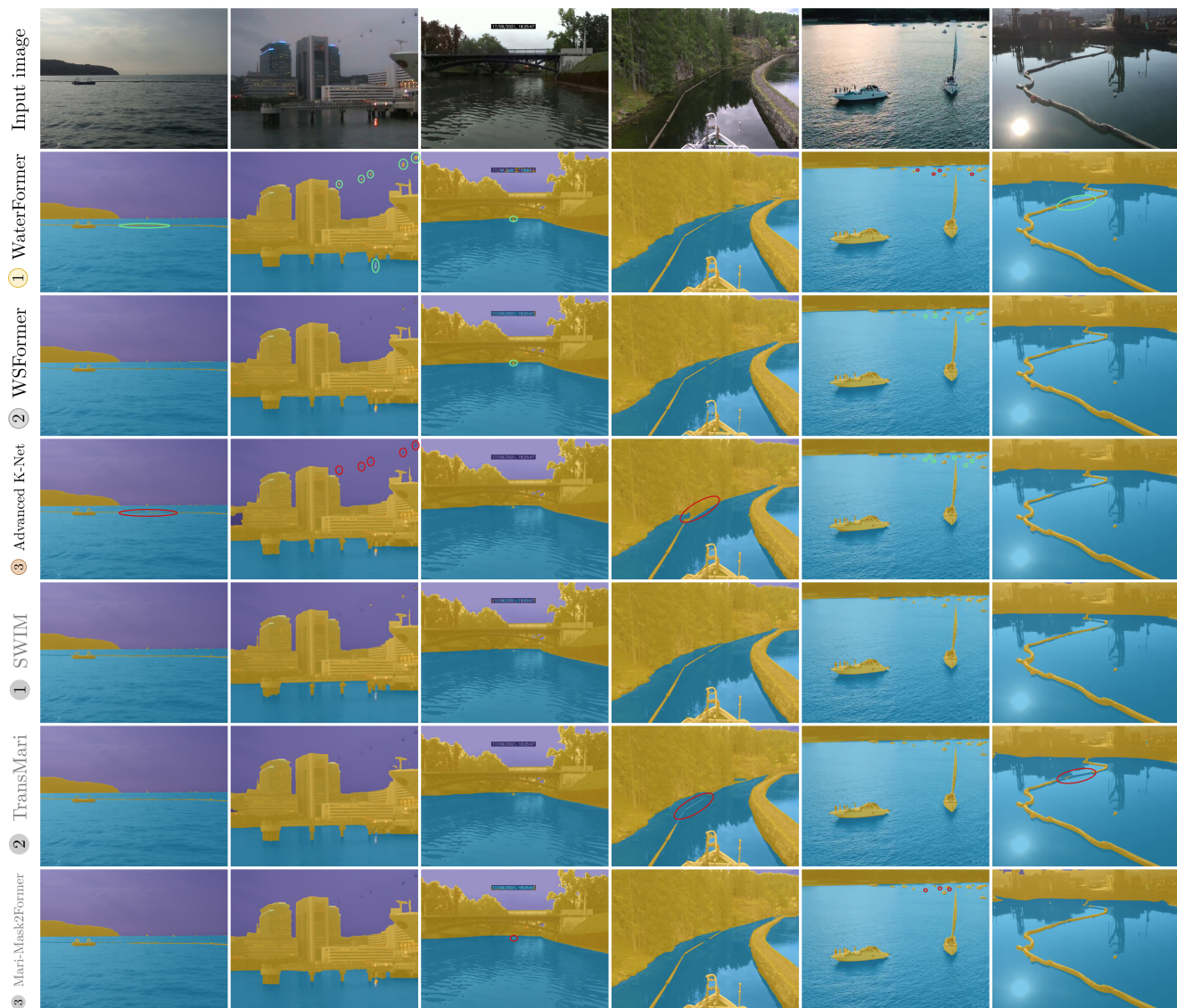
Figure 8: Qualitative comparison of methods for USV-based Obstacle Segmentation. Prominent errors and examples of good behaviour are highlighted in red and cyan, respectively.

on WaterScenes dataset [79], then fine-tuned on LaRS. Test Time Augmentation was used for producing the final predictions. Advanced K-Net was only trained on LaRS data, using K-Net and a SWIN-L backbone. Lion [12] was used instead of Adam for optimizing the model parameters.

Detection by scene attributes: Figure 6 shows the performance with respect to scene attributes, including environment type, illumination, amount of reflections and scene conditions. Overall, the top three methods outperform the previous challenge winners in most categories, particularly in challenging scenarios such as heavy reflections, foggy scenes and plants or debris presence in water. It should be noted that the second best performing method, WSFormer

performs best for many specific attributes, such as night-line illumination, heavy reflections, sun glitter, rain, and fog.

Performance by obstacle size: Figure 7 compares the detection performance of the top three methods and the previous challenge winners across different obstacle sizes. The largest differences between methods are revealed on small obstacles, with the winning method WaterFormer outperforming all others by a quite large margin for very small obstacles. We can also observe that the second best performing method WSFormer produces the fewest false positives for small obstacles, however that comes at a price of detecting fewer obstacles overall.

Qualitative results: Examples of predicted scene seg-

Table 3: Results for the USV-based Embedded Obstacle Segmentation Challenge. Methods faster than ≥ 30 FPS on the target device OAK4 are considered (denoted in teal) when determining the final rankings. For evaluation comparison, we include the winning method from the non-embedded challenge from Section 3.2 at the top and last year's [35] winning methods as a baseline, but do not consider them as part of the challenge (denoted in gray). Only the best valid submission from each team is reported. The best results from considered methods are denoted in bold.

Place	Institution	Method	Section	FPS	Q↓	μ	Pr	Re	F1	mIoU
	GIST AI Lab	*WaterFormer*	B.1	1.7 (RTX 4090)	83.2	80.5	81.6	88.0	84.7	98.3
①	DLMU	RSOS-Net	C.1	85.1	**64.2**	**72.5**	**66.4**	67.9	**67.1**	95.7
②	ACVLab	EFFNet	C.2	56.3	62.3	71.3	61.1	68.0	64.4	**96.7**
	EAIC-UIT	eWaSR-RN50	[35]	103.4	55.3	68.5	48.5	70.5	57.4	96.2
	DLMU	Mari-MobileSegNet		60.3	51.3	69.1	55.7	52.2	53.9	95.3
③	EAIC-UIT	eWaSR-RN101 p2		50.3	41.6	71.1	34.3	60.9	43.8	94.9
	FarmLabs	PIDNet-Large		21.2	41.0	57.6	40.2	61.5	48.6	84.3

mentations are presented in Figure 8. We can observe that all the depicted methods interpret the majority of the scene very well, the main differences appearing in the predictions for very small, thin or ambiguous objects, such as the strong reflection in column 2 or the thin structures in columns 1, 4, and 6. WSFormer and Advanced K-Net methods also perform very well on tiny buoys in column 5.

3.2.3 Discussion and Challenge Winners

The overall winners of the USV-based Obstacle Segmentation challenge are:

1st place: GIST AI Lab with WaterFormer,

2nd place: Multi-institution team (Yancheng Institute of Technology, Hong Kong University of Science and Technology, University of Liverpool, Xi'an Jiaotong-Liverpool University) with WSFormer, and

3rd place: Independent researcher with Advanced K-Net

All three methods outperformed the previous challenge's winner on the LaRS benchmark and show notable improvement, especially with regard to very small objects, thin structures, and low-light circumstances. However, a large number of tiny objects and visually ambiguous appearances remain open issues. We expect the performance will continue to improve with new datasets and newer methods.

3.3. USV-based Embedded Obstacle Segmentation

Modern obstacle detection methods often depend on high-performance, energy-intensive hardware, making them unsuitable for small, energy-constrained USVs [63]. The USV-based Embedded Obstacle Segmentation challenge aims to address this limitation by encouraging development of innovative solutions and optimization of established semantic segmentation architectures which are efficient on embedded hardware. The challenge builds on the success of last year's challenge [35] and is an extension of the USV-based Obstacle Segmentation task outlined in Section 3.2. Submissions are evaluated and benchmarked on a real-world OAK4 device from Luxonis.

3.3.1 Evaluation Protocol

To ensure compatibility with embedded devices, we impose additional constraints that must be adhered to during the development and submission phases like in [35]. Submissions must follow:

- *Static Graph* – Neural networks must have a well-defined static graph and fixed shapes, and must be exportable to ONNX format without custom operators.

- *Operation Support* – ONNX can contain only a specific set of operations constrained by the hardware, details of which we provide before the start of the challenge.

- *Standardized inputs and outputs* – Models are evaluated directly on the device, so they must accept fixed-size input images (768×384) normalized using ImageNet [16] mean and standard deviation. Output must be a single-channel 2D segmentation mask containing per-pixel class indices. Only methods with a single image input and a single output are permitted.

- *Performance Requirement* – Models must achieve a throughput of at least 30 FPS on the embedded device OAK4.

Submitted architectures are quantized to INT8 using the validation set of LaRS [86] and leveraging Qualcomm's SNPE toolkit [55]. The models are then compiled into a binary executable for the target hardware. During inference,

the input images are resized, centered, and padded to a 768×384 resolution with the maintained aspect ratio, and the outputs are resized to match the original image resolution. The final scores are computed using the same evaluation protocol described in 3.2.1. In addition to the LaRS metrics, the average throughput achieved on the embedded device is also reported.

3.3.2 Submissions, Analysis and Trends

The embedded obstacle segmentation challenge received 26 submissions from 4 different teams. In addition, we consider the winning method from last year's competition. We show the best submission from each team in Table 3. For final rankings, we only consider submissions from this year which are faster than 30 frames per second. We received submission reports for the 2 winning methods.

Both RSOS-Net (C.1) and EFFNet (C.2) prioritize lightweight architectures and efficient real-time inference leveraging ResNet [28] backbones. RSOS-Net excels at balancing speed and accuracy, while EFFNet explores ensemble techniques to enhance prediction robustness.

RSOS-Net (Section C.1) features a ResNet-101 backbone paired with a lightweight decoder employing separable convolutions and an attention-based fusion module. Its Fast Pyramid Pooling Module (FPPM) enhances the receptive field, effectively distinguishing obstacles from surface disturbances. EFFNet (Section C.2) utilizes an ensemble of two models – ResNet-50 and ResNet-101 backbones combined with DeepLabv3+ [11] decoders. Prolonged training improved performance, while additional augmentations or heavier backbones did not. The method emphasizes multiscale feature extraction and stability after quantization. No additional data is used in both methods and they are trained only on the LaRS [86] dataset.

Both winning methods significantly outperformed last year's winner and baseline method eWaSR-RN50 (+8.9 Q and +7.0 Q for RSOS-Net and EFFNet, respectively). At a small cost in recall (-2.6% and -2.5%), precision was significantly better ($+17.5\%$ and 12.6%). Both methods were slower (85.1 FPS and 56.3 FPS for RSOS-Net and EFFNet, respectively) than baseline (103.4 FPS eWaSR-RN50) but still achieved high throughput and are suitable for embedded device deployment. We provide full quantitative results in Table 3.

Additionally, we compare the three winning methods under various environmental conditions. For readability, we only include the most interesting results in Figure 9. As expected, both RSOS-Net and EFFNet significantly outperform other methods in various scenarios. However, RSOS-Net and EFFNet mostly differ in a few key areas. RSOS-Net is considerably better in the presence of heavy reflections. It also outperforms EFFNet under challenging conditions, such
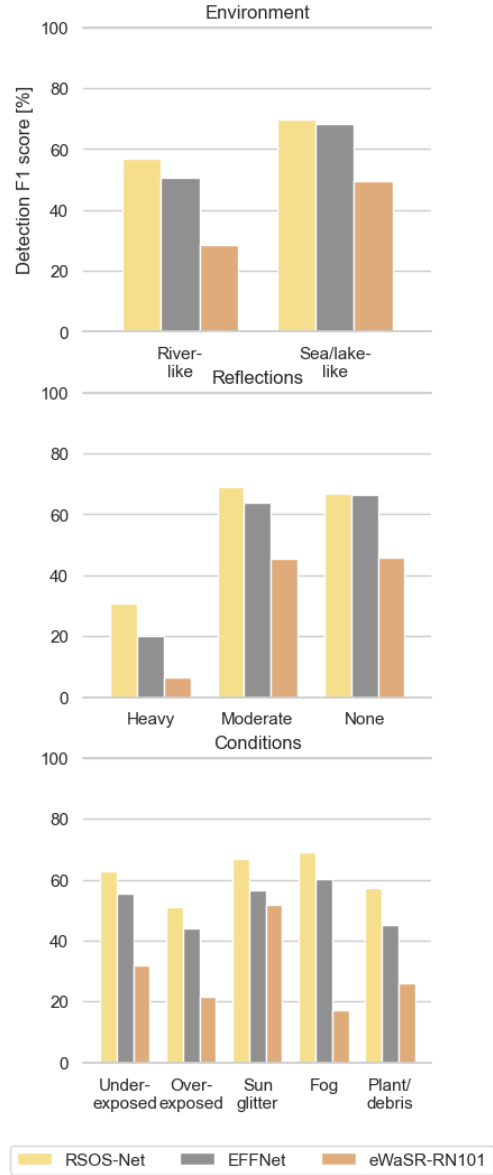

Figure 9: Comparison of F1 detection score for the best 3 submissions from Section 3.3 under various environmental conditions (environment type, reflections, and conditions).

as over or under-exposure, glitter, fog, and plant debris. The latter could be a reason for the slightly better performance of RSOS-Net in river-like scenes.

We further qualitatively compare the best 3 submissions in Figure 10. RSOS-Net indeed outperforms EFFNet under conditions discussed in the previous paragraph. We can see it performs better in the presence of reflections and during night. While all methods are capable of detecting small objects like buoys, they are still limited by the fixed input shape requirement and at times struggle to detect small ob-

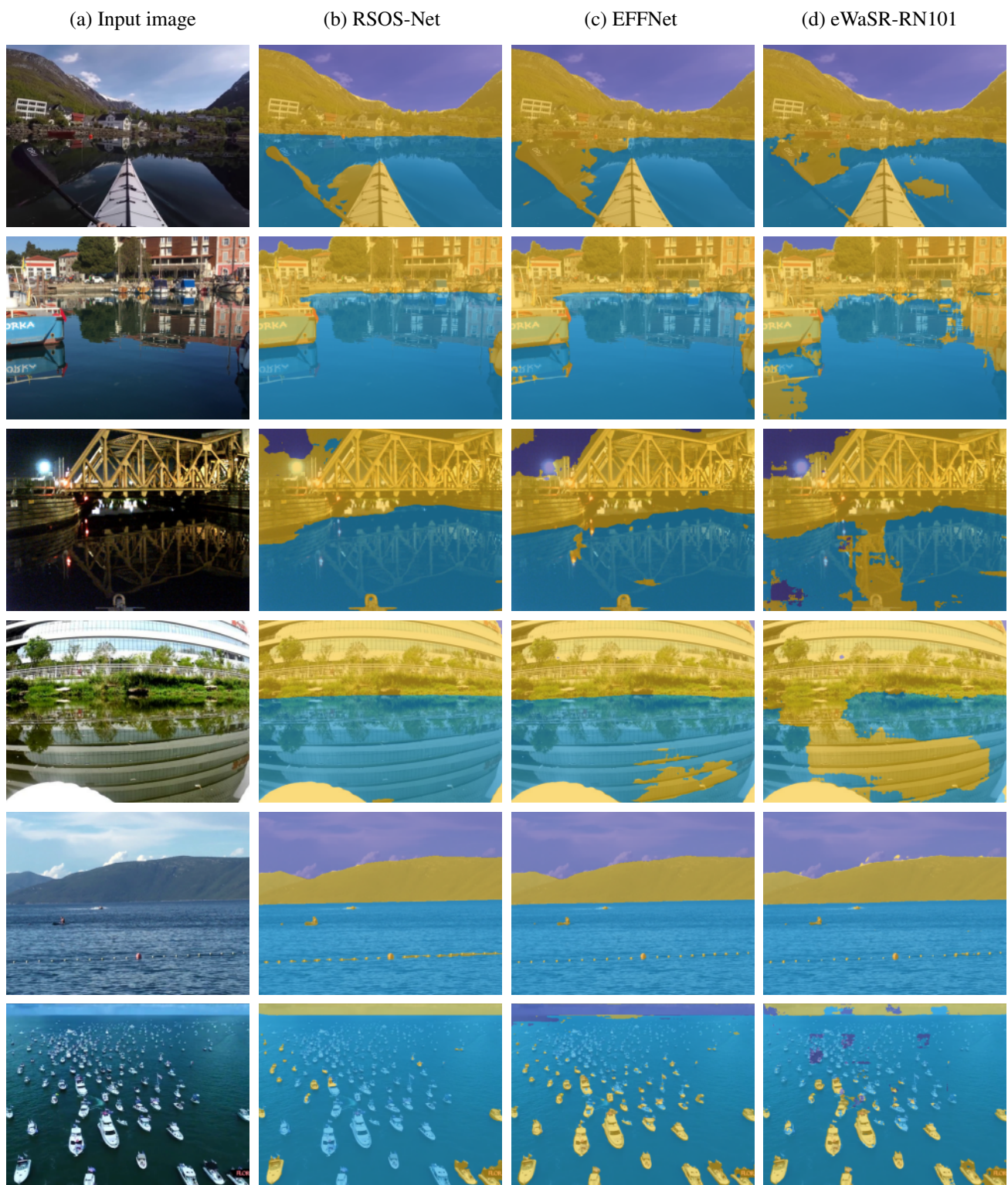| (a) Input image	(b) RSOS-Net	(c) EFFNet	(d) eWaSR-RN101

Figure 10: Qualitative comparison of the best 3 submissions for USV-based embedded obstacle segmentation from Section 3.3.

jects when multiple are present in the scene.

3.3.3   Discussion and Challenge Winners

The overall winners of the USV-based Embedded Obstacle Segmentation are:

1ⁿᵈ place: Dalian Maritime University (DLMU) with RSOS-Net.

2ⁿᵈ place: Advanced Computer Vision Lab (ACVLab) with EFFNet, and

3ʳᵈ place: University of Information Technology, VNU-HCM (EAIC-UIT) with eWaSR-RN101 p2.

The 2 best-performing submissions significantly outperformed winning methods from last year, while maintaining above real-time throughput. Submitted methods adapt better to challenging scenarios such as glitter, reflections, and lightning. However, due to fixed input shape requirements, they still perform worse in the presence of many small obstacles, especially compared to regular segmentation track. We leave this open for future competitions.

3.4. USV-based Panoptic Segmentation Challenge

This year MaCVi introduced a new panoptic sub-challenge based on the recent LaRS dataset [86]. In contrast to our segmentation challenges, the panoptic challenge calls for a more fine-grained parsing of USV scenes, including segmentation and classification of individual obstacle instances. This formulation encapsulates the requirements of scene parsing for USV navigation in a more principled way, paving the road for downstream tasks such as tracking individual obstacles, trajectory prediction and obstacle avoidance.

The task of the USV-based Panoptic Segmentation Challenge was to develop a panoptic segmentation method that parses the input USV scene into several background (*i.e.* stuff) and foreground (*i.e.* things) classes and outputs a set of instance masks and their class labels. Stuff classes include water, sky and static obstacles, and thing classes include 8 different types of dynamic obstacles – boat/ship, buoy, row boat, swimmer, animal, paddle board, float and other. In addition to training on the LaRS training set, which uses the aforementioned classes, participants were allowed to use other datasets for (pre-)training if disclosed.

3.4.1   Evaluation protocol

The panoptic performance of submitted methods is evaluated using standard panoptic performance evaluation measures [37,86]: segmentation quality (SQ), recognition quality

(RQ) and the combined panoptic quality (PQ):

$$PQ = \underbrace{\frac{\sum_{(p,g)\in TP} IoU(p,g)}{|TP|}}_{\text{segmentation quality (SQ)}} \times \underbrace{\frac{|TP|}{|TP| + \frac{1}{2}|FP| + \frac{1}{2}|FN|}}_{\text{recognition quality (RQ)}}.$$
(1)

To determine the ranking of the submitted methods, overall panoptic quality (PQ) was considered. For additional insights, individual metrics are also reported separately for *thing* and *stuff* classes indicated by superscripts $(\cdot)^{Th}$ and $(\cdot)^{St}$.

Following [86], additional dynamic obstacle detections inside static obstacle regions are not considered as false positives. Finally, every participant was required to submit information about the speed of their method including the hardware used for benchmarking and the measured speed in frames-per-second (FPS).

3.4.2   Submissions, Analysis and Trends

The USV-based Panoptic Segmentation Challenge received 21 submissions in total from 7 different teams. We only analyze the best-performing method of each team as per the rules of the challenge. Results of the remaining submitted methods are available on the public leaderboards of the challenge on the MaCVi website [36]. In Table 4 we report the overall results and final standings of the best methods submitted by each team. The MaCVi team also contributed a baseline Mask2Former (Swin-B) method [13] for comparison. Additionally, a recent PanSR method [85] was submitted to the challenge by the MaCVi team, but is not considered for the winning positions of the challenge. In this section we analyze all the contributed methods, with a special focus on the top three approaches. Short descriptions of the top three methods and baseline approaches are also available in the Appendix D.

We are happy to report that all the teams contributed strong methods and improve over the baseline Mask2Former method by a significant margin. Specifically, the first-placing MaskDINO method [40] achieves a PQ of 53.9, outperforming the baseline by +12.5 % PQ. While not considered for winning the challenge, the top-performing PanSR method boosts performance by an additional +3.4 % PQ.

Interestingly, the top three methods take a vastly different approach to the problem, but reach similar performance. The (#3) method utilizes an open-vocabulary CLIP-based method [81], the (#2) method combines a top-performing segmentation network from the Obstacle Segmentation Challenge (Section 3.2) with an instance segmentation network [7] for addressing thing classes, and the (#1) method utilizes a strong detection-optimized panoptic network [40], while also experimenting with an open vocabulary approach. None of analysed methods utilized addi-

Table 4: Results for the USV-based Panoptic Segmentation Challenge measured in overall panoptic quallity (PQ) and separate for thing and stuff classes. Competing methods are compared to a baseline Mask2Former model [13] and the top-performing PanSR method [85]. *The throughput of methods, measured in frames-per-second (FPS), is self-reported by the authors.

| Place	Team	Method	Section	Hardware	FPS*	PQ	PQ_{th}	PQ_{st}
★	MaCVi Team	PanSR (Swin-L)	§D.4	RTX A4500	0.7	**57.3**	**43.0**	95.4
①	Fraunhofer IOSB	MaskDINO	§D.1	V100	1.0	53.9	39.4	92.3
②	GIST AI Lab	PanopticWaterFormer	§D.2	H100	1.1	53.0	37.3	94.7
③	UL 1	FC-CLIP-LaRS	§D.3	A100	10	49.7	32.4	**95.6**
4th	WaterScenes	WaterScenes	-	RTX 4090	10	48.6	31.2	95.1
5th	YCIT	SeeDroneSee	-	H100	4.8	47.7	30.0	95.0
6th	XJTLU	Mask	-	RTX 3090	1.7	47.4	29.5	94.9
7th	UL 2	PSAM	-	RTX 2080 Ti	0.6	46.2	28.9	92.1
-	MaCVi Team	Mask2Former (Swin-B)	-	V100	4.8	41.4	22.3	92.5
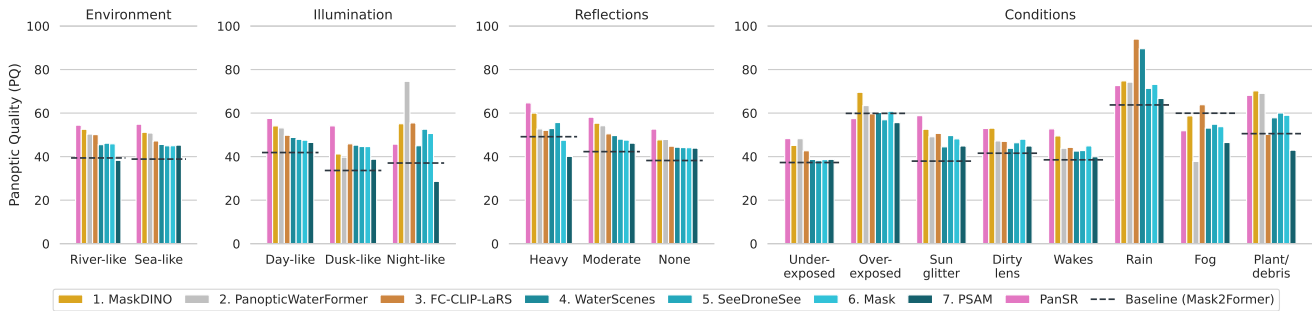
Figure 11: USV-based Panoptic Segmentation: Performance of top methods in terms of panoptic quality (PQ) w.r.t. different scene attributes. The performance of the baseline method (Mask2Former [13] w/ Swin-B) is marked as a dotted line for reference.
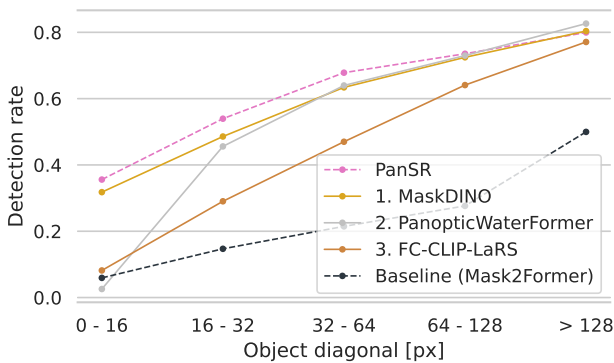

Figure 12: USV-based Panoptic Segmentation: Dynamic obstacle detection rate of top methods with respect to ground-truth obstacle size.

tional data during training other than standard pre-training datasets (COCO [42]). In the following, we analyze the top-performing methods of each of the teams in more detail.

Detection by scene attributes: In Figure 11 we compare the performance of methods with respect to scene attributes, including environment type, illumination, amount of reflections and scene conditions. Overall, all submited methods outperform the baseline (Mask2Former [13]) in most categories. The top performing methods also demonstrate great stability across different scenarios. On several exceedingly rare scene attributes ($< 5\%$) such as night-like illumination, rain and fog, performance of methods is less consistent with overall trends. For example, on night-time scenes the (#2) method PanopticWaterFormer achieves the best performance, also visible in the qualitative examples (Figure 13).

Performance by obstacle size: Figure 12 compares the detection performance of the top three methods with the Mask2Former baseline [13] and the top-performing PanSR method [85] across different obstacle sizes. As expected, the largest differences between methods are revealed on small obstacles. Specifically, PanSR and the (#1) MaskDINO method offer a major boost in the detection rate on the smallest obstacles compared to other methods.

Qualitative results: Examples of panoptic method predictions for top methods are shown in Figure 13. Compared
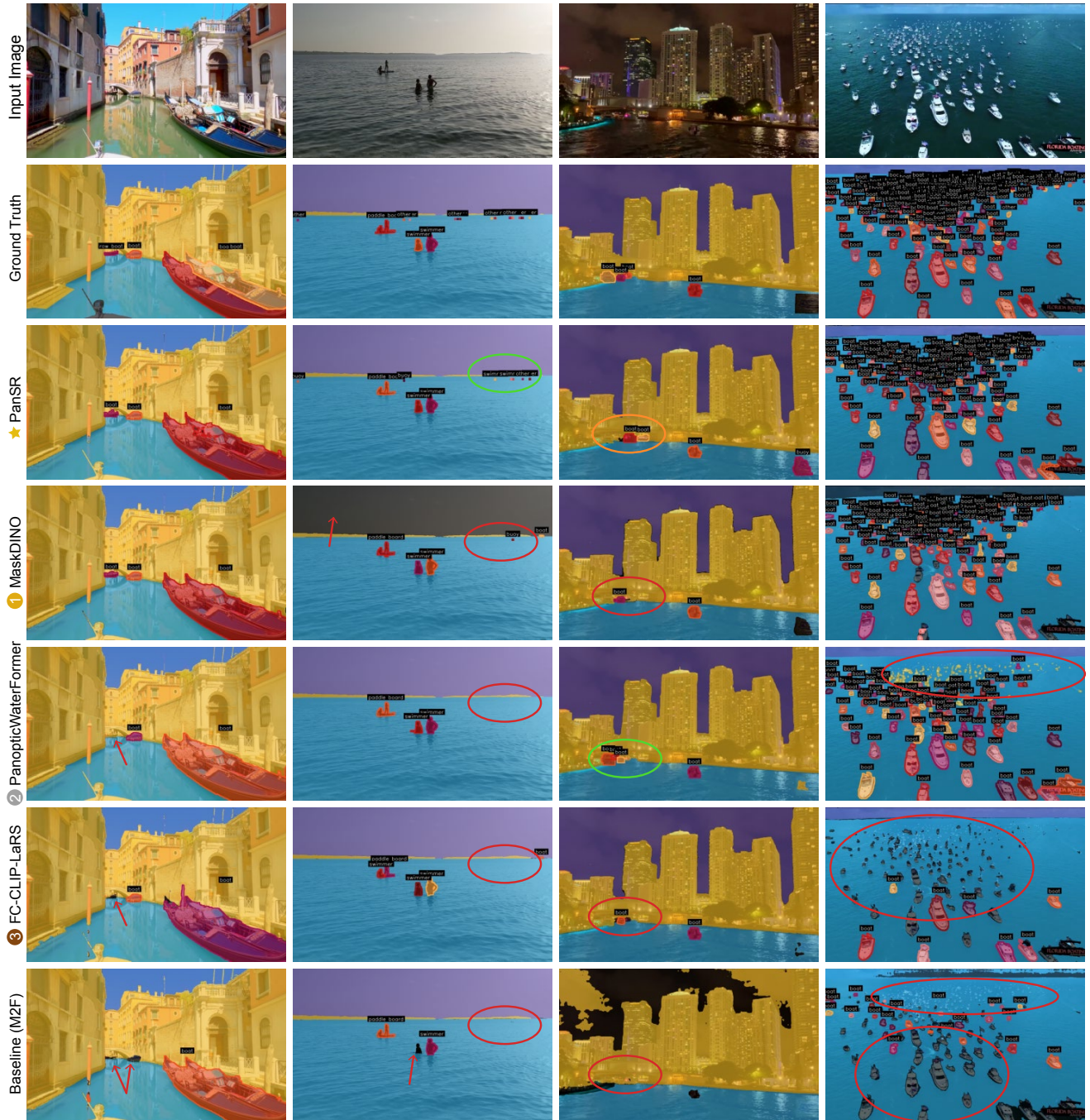
Figure 13: USV-based Panoptic Segmentation: Qualitative comparison of top 3 ranking methods.

to the baseline (Mask2Former) all methods improve the segmentation quality and detect a larger percentage of dynamic obstacles. The largest differences between methods are observed on small obstacles (column 2 and 4) and in crowded scenes (column 4), where (#1) MaskDINO and especially PanSR perform significantly better.

3.4.3 Discussion and Challenge Winners

The overall winners of the USV-based Panoptic Segmentation challenge are as follows:

1st place: Fraunhofer IOSB with MaskDINO,

2nd place: GIST AI Lab with PanopticWaterFormer,

3rd place: University of Ljubljana 1 with FC-CLIP-LaRS

Although using very different approaches, all three methods outperformed the baseline method on the LaRS benchmark and show notable improvement, especially with regard to segmentation quality and detection of small objects. However, these methods still struggle in the case of crowded scenes, very small objects and rare cases or conditions. The recent PanSR method [85] already demonstrates that architectural and training choices can make a large impact on the detection performance on crowded scenes and small objects. Furthermore, some teams experimented with an open-vocabulary approach, which shows potential for addressing rare cases by harnessing language-grounded knowledge from large-scale data.

4. MarineVision Restoration Challenge

Underwater image restoration [17, 19–21] is the process of enhancing the visual quality of images captured in aquatic environments by eliminating degradations caused by light absorption and scattering. These degradations reduce contrast and introduce color casts, making object detection and localization of underwater species a challenging task. Restoring lost visibility and improving color balance aid in the detection and localization of underwater species, facilitating tasks such as biodiversity monitoring, marine conservation, and underwater robotics. The MarineVision Restoration Challenge (MVRC) focuses on developing robust image restoration methods to enhance the detection and localization of underwater species. In the first edition of the MVRC challenge the participants are provided with the RSUIGM dataset [18]. The dataset consists of 30 ground truth scenes and 200 corresponding synthetically generated degraded observations for each scene. The challenge is divided into two steps: in the first step, participants must develop a robust algorithm for restoring the degraded images; in the second step, participants must perform the detection and localization of the underwater species considering the restored images from the first step. Participants are permitted to utilize other publicly available datasets to enhance underwater image restoration.

4.1. Evaluation Protocol

The evaluation is conducted in two phases. In the first phase, we consider perceptual quality metrics (PQM)– Underwater Image Quality Metric (UIQM), Underwater Color Image Quality Evaluation (UCIQE), Colorfulness Contrast Fog density index (CCF) to assess the performance of restoration methods. In the second phase, we consider Mean IoU (mIoU), F1 Score, and mean Average Precision (mAP) performance metrics to evaluate the effectiveness of the detection (OD) and localization methods. Further, we compute

the overall score Q as shown below:

$$Q = 0.8 \left(\frac{\text{CCF} + \text{UIQM} + \text{UCIQE}}{3} \right)$$
$$+ 0.2 \left(\frac{\text{F1 score} + \text{mAP} + \text{mIoU}}{3} \right) \quad (2)$$

Note: The CCF metric does not have a defined range of values. Therefore, we normalize CCF values between 0 and 1 for fairness and ease of evaluation. We emphasize more on perceptual enhancement of the images and showcase marine species detection as a downstream application of underwater image restoration, hence the weightage (80%) for perceptual metrics and (20%) for object detection evaluation metrics.

4.2. Submissions, Analysis and Trends

In the first edition of the challenge, we received over 40 submissions from 8 different teams. The top performing teams are reported in Table 5. The top 4 teams were invited to submit the description of their methods, which are provided in sections E.1, E.2, E.3, E.4 respectively. The submissions show the authors refer to a wide variety of models and approaches for underwater image restoration and enhancement. Team (#1) NJUST-KMG adopt a two-stage pipeline for underwater image enhancement. The authors first restore the underwater images using HVI-CIDNet and to further remove the hazy effect in the images, the authors employ dehazing methods CasDyF-Net and SCANet. Followed by restoration and enhancement, the authors perform marine species detection using pre-trained version of DETR object detection model. In contrast other teams (#2) BUPT, (#3) MTU, and (#4) ACVLab use end to end approaches for underwater image restoration and enhancement followed by object detection. Team (#2) BUPT, build upon the existing NAFNet with a frequency separation and fusion block aimed at processing high and low frequency details separately. While teams (#1) and (#2) adopt deep learning approaches, team (#3) adopt statistical method, Texture Enhancement Model Based on Blurriness and Color Fusion (TEBCF) to restore degraded underwater images. TEBCF is a non-data driven method, requires no pre-training and can be directly used for inferencing. Followed by restoration, the authors use pre-trained YOLO-NAS model for detecting marine species in the restored underwater images. The qualitative comparison of under image restoration methods proposed by top performing teams in shown in Figure 14.

4.3. Discussion and Challenge Winners

The winners of the challenge are as follows:

1st place: Nanjing University of Science and Technology

2nd place: Beijing University of Posts and Telecommunications, Beijing, China with MCPRL
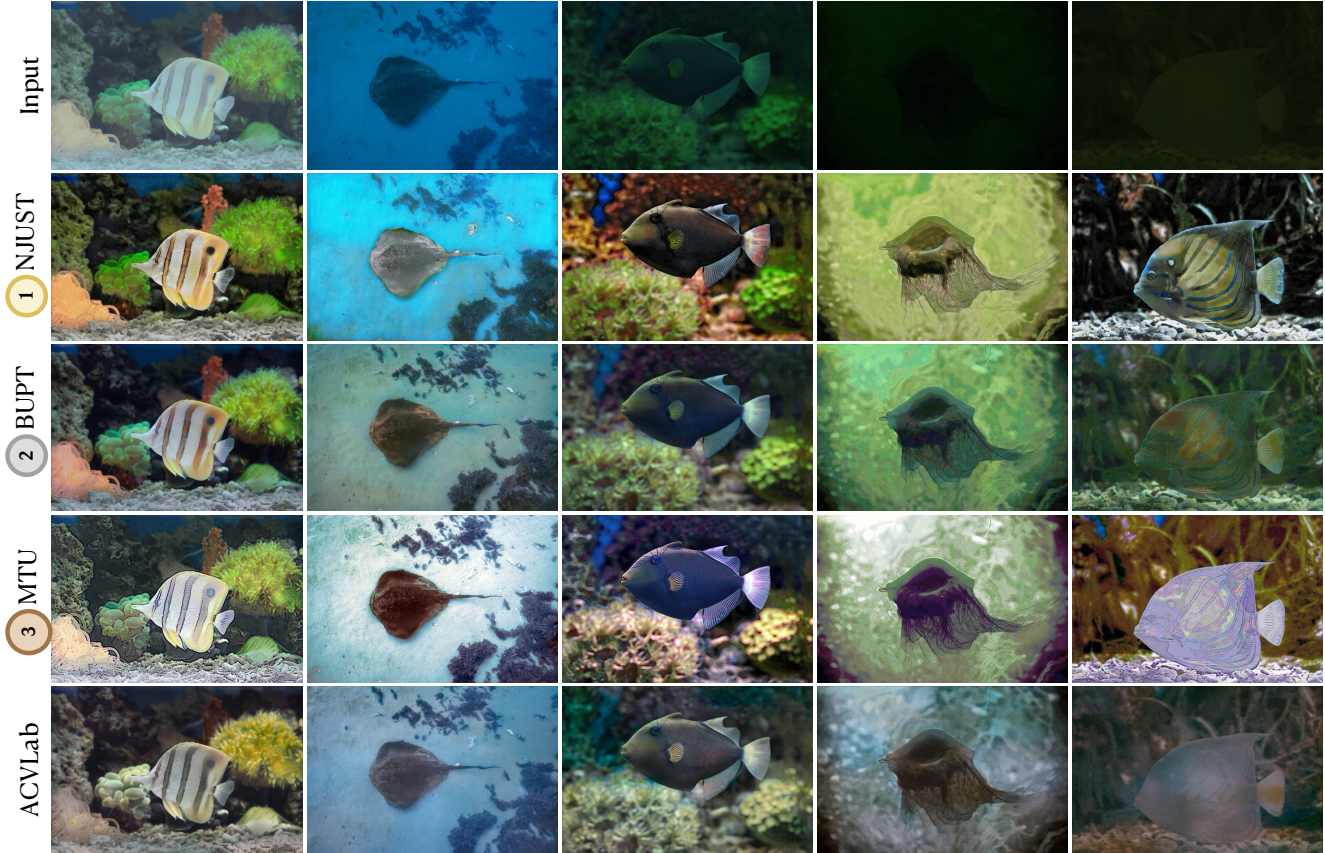
Figure 14: Qualitative comparison of underwater image restoration proposed by top performing teams in MarineVision Restoration Challenge.

Place	Team	Method	Section	Hardware	UIQM	UCIQE	CCF	mIoU	F1	mAP	PQM	OD	Final Score
1	NJUST-KMG	NJUST-KMG	§E.1	RTX 3090	0.70	0.57	0.08	0.69	0.13	0.13	0.45	0.31	0.42
2	BPUT MCPRL	BUPT MCPRL	§E.2	RTX 4090	0.37	0.53	0.02	0.64	0.16	0.16	0.31	0.32	0.31
3	MTU	MTU	§E.3	Tesla V100	0.00	0.60	0.01	0.64	0.16	0.16	0.20	0.32	0.23
4	ACVLab	Color Transfer Fusion Network	§E.4	RTX 2080 Ti	0.00	0.50	-0.01	0.54	0.14	0.14	0.16	0.27	0.18

Table 5: Quantitative comparison of methods proposed by top teams in MarineVision Restoration Challenge. The final score is measured as the weighted average of Perceptual Quality Metrics (PQM) and Object Detection (OD) metrics.

3rd place: Michigan Technological University, USA

All the Top Three teams outperformed the set baselines for underwater image restoration task. Team (#1) demonstrated a two-stage pipeline for restoration–image restoration followed by haze removal, significantly improving the performance in the detection of marine species. In contrast, Team (#3) showcased a non-learning-based algorithm for underwater image restoration. However, the resulting images consist of sharp edges in all images, indicating the need for better restoration models.

5. Conclusion

In this summary paper, we analyzed the challenges of the 3rd Workshop on Maritime Computer Vision. Specifically,

MaCVi 2025 hosted four different surface domain maritime challenges, and one underwater image restoration challenge.

The USV-based Object Distance Estimation challenge focused on detecting buoys in image space and their metric distances in world space. The top two submission significantly outperformed the baseline yielding insights into backbone selection and loss function balance. In future versions, it might be interested to see the more complicated multi-class or open vocabulary distance estimation setups.

USV-based Obstacle Segmentation Challenge addressed semantic scene parsing for USVs with a focus on obstacle detection and saw significant improvements over submissions of the previous iteration of MaCVi.

USV-based Embedded Segmentation Challenge evalu-

ated method on the same task, but running it on real-world embedded hardware and all its limitations. While still far from the unbounded state-of-the-art, this year's methods substantially reduced the performance gap at impressive, more than real-time speeds, and are quickly catching up to the top-performing methods.

USV-based Panoptic Segmentation featured a much more difficult panoptic task, which requires methods to detect, segment and classify also individual instances of dynamic obstacles in the scene. All participants significantly outperformed the strong baseline we set at the start of the challenge and made large leaps in tackling major challenges of the task, such as the detection of very small obstacles and robustness to variation in scene conditions.

The First Edition of the MarineVision Restoration Challenge addressed the complex task of underwater perception. The challenge provided synthetic data that largely resembled the real-world optical properties of water pertaining to diverse geographical locations. The task involved restoration of images and the perform marine species detection on the restored images as a downstream application useful in tasks such as marine life health monitoring and conservation, perception for underwater vehicles such as submarines and ships. All participants outperformed the set baselines for the underwater image restoration task.

Overall, the challenges presented at MaCVi 2025 featured strong entries across the board, pushing the boundaries of what is possible in maritime vision in several different aspects, while outlining multiple exciting future research directions for the field.

Appendix - Submitted Methods

A. Supervised Object Distance Estimation

A.1. ① Data Enhance

Zhiqiang Zhong, Zhe Zhang, Sujie Liu, Xuran Chen, Yang Yang
Nanjing University of Science and Technology
{zhongzhiqiang2002, zhe.zhang, xuran_chen, yyang}@njust.edu.cn, sruis1109@163.com

This report presents the solution to the Approximate Supervised Object Distance Estimation challenge at the 3rd Workshop on Maritime Computer Vision. We use the YOLOv7 base model, enhancing it with an additional detection head and the BiFormer attention mechanism to better focus on small objects. Additionally, we increase the sample size by horizontally flipping images and apply a range of data augmentation techniques to improve the model's performance. We also integrate the SimAM attention mechanism to further enhance detection performance. Ultimately, we achieve a score of 0.2719, securing first place.

Introduction: We focus on several key areas, including multimodal machine learning, open-environment machine learning, and incremental [75, 76, 78]. This challenge involves developing algorithms for estimating the distance to buoys from monocular images.

Method: This section provides an overview of our approach. Our method is built upon the YOLOv7 model and primarily includes data augmentations, an additional detection head, the BiFormer attention and the SimAM attention.

- **Data Augmentations:** We increase the sample size by horizontally flipping the images and enhance the model's performance and robustness using a range of data augmentation techniques, including image rotation, translation, scaling, shearing, perspective transformation, vertical and horizontal flipping, mosaic, mixup, and copy-paste.

- **Additional Detection Head:** YOLOv7 is an anchor-based object detection model, rather than anchor-free. Therefore, we add a small initial anchor box and incorporate an additional detection head to detect small objects in the image.

- **BiFormer:** BiFormer [44] is an innovative attention mechanism that enhances the model's detection performance by simultaneously capturing both local and global features through a dual-layer routing design. During the feature extraction process, BiFormer computes attention for each local region to capture detailed features. This step improves the model's sensitivity to small objects and fine details, thereby enhancing detection accuracy. We integrate BiFormer Attention as a plugin into YOLOv7. Specifically, we add BiFormer Attention at the end of the SPPCSPC module and also at the end of the Conv module.

- **SimAM:** SimAM [74] is a parameter-free attention mechanism inspired by neuroscience that assigns 3D attention weights to feature maps in a flexible manner, without increasing model complexity. This enables more efficient and lightweight processing. By using an energy function to measure the linear separability between neurons, SimAM identifies and prioritizes important neurons, thereby enhancing feature extraction. We integrate SimAM into a modified YOLOv7 model to improve object detection performance, leveraging its

ability to achieve attention without the need for additional parameters.

Experiments: The object distance estimation dataset comprises about 3,000 images of maritime navigational aids, mainly featuring red and green buoy markers. Only the training set is provided, while the test set is withheld to benchmark model performance in the competition. We train the model using an NVIDIA GeForce RTX 3090, with the number of 400. The experimental results are shown in the table below.

Method	Scores
yolov7	0.2260
+ augmentations	0.2488
+ augmentations + additional head	0.2611
+ augmentations + additional head + biformer	0.2680
+ augmentations + additional head + biformer + simam	0.2692
+ augmentations + additional head + biformer + simam + flip images	0.2719

A.2. ② YOLOv7 Depth - Widened

Matej Fabijanić, Fausto Ferreira
University of Zagreb Faculty of Electrical Engineering and Computing
`{matej.fabijanic, fausto.ferreira}@fer.hr`

Our method is based on the YOLOv7 architecture provided by the MaCVi 2025 Distance Estimation Challange organizers, which was already customized to include metric distance estimation for detected objects. Our primary contribution was further enhancing the architecture by increasing its width to improve performance.

We increased the model's capacity by modifying the *width_multiple* parameter, which scaled up the number of feature channels in each layer, leading to a total of approximately 49 million parameters. We utilized the default training configuration provided by the organizers with a few key adjustments. Specifically:

- **Optimization:** The distance loss function was weighted, doubling the loss when the ground-truth object distance was below 441 meters. We have also changed the model fitness calculation to consider only the mAP@50:95 metric as that was the metric scored for the challenge.

- **Augmentation:** We employed HSV (hue-saturation-value) augmentation, left-to-right flipping with a 50% probability, and increased the scale parameter to 2.0, which significantly improved model performance.

Our model was trained solely on the dataset provided by the challenge organizers. The training set comprised 95% of the images, with the remaining 5% reserved for validation. No external datasets or pre-trained weights were used. This resulted in 2793 images used for training and 147 images used for validation. However, we first trained the custom YOLOv7

model until weight convergence without considering the relative distance error, only training for object detection like a standard YOLO. We then used this converged model as the starting point when training for both object detection and metric distance estimation.

Training was performed on 2x Nvidia GTX 1080 GPUs. The inference speed of the model was approximately 0.15 seconds per image.

During analysis, we observed challenges such as the difficulty of detecting distant buoys and markers due to resolution limitations, vessel motion, and adverse visibility conditions. These observations inspired adaptations like the increased scale parameter to focus on the central, more informative parts of the images.

Empirical testing revealed that increasing the scale factor provided the largest model performance boost regarding mAP50-95 metric and relative distance loss metric. This adaptation aligns with the dataset characteristics, where objects of interest are typically near the image's center.

One of the first ideas was to go through the provided dataset and check if the annotations needed corrections to make the bounding boxes fit more "tightly" on the objects, especially the farther ones. However, modifying the annotations and training on "tighter" bounding boxes severely decreased performance on the hidden test dataset, even though the model achieved higher mAP50-95 and lower relative distance error numbers on the modified data. This suggests that adding another expected output to the YOLOv7 architecture might lead to easier overfitting during training.

A.3. Baseline methods

MaCVi Organizers

We include a slightly adapted method from [34] as baseline method.

B. USV-based Obstacle Segmentation

B.1. ① WaterFormer

Seongju Lee, Junseok Lee, Kyoobin Lee
`{lsj2121, junseoklee,`
`kyoobinlee}@gm.gist.ac.kr,`
Artificial Intelligence Laboratory at Gwangju Institute of Science and Technology (GIST)

Method. We introduce *WaterFormer*, a model for USV-based obstacle segmentation illustrated in Figure 15, which leverages parameter-efficient fine-tuning of vision foundation models using adapters. Specifically, we used Mask2Former [13] with the DINOv2 (Large) [52] backbone. We inserted an adapter with an FC(1024, 128)-GELU-DC-GELU-FC(128, 1024) architecture between the DINOv2 layers, where FC(a, b) is a fully connected

layer that takes an a-D feature as input and outputs a b-D feature, GELU is the Gaussian Error Linear Unit [29], and DC is deformable convolution [71]. During training, the weights of DINOv2 layers are frozen. Our implementation is based on the MMSegmentation framework [1].

Training Details. For training, AdamW [50] optimizer was employed with a learning rate of 0.0001, a weight decay of 0.05, epsilon set to 10^{-8}, and betas set to (0.9, 0.999). The batch size was set to 8, and the training iterations were set to 40,000. The augmentations included random resizing with scales defined by `[int(512*x*0.1) for x in range(5, 21)]`, using the shortest edge of the image as a standard and a maximum size of 2048. This was followed by random cropping with a defined size of 512 × 512 pixels, random horizontal flipping with a 50% probability, and photometric distortions to introduce visual variation.

Datasets and Pretrained Weight. We used only the LaRS [86] dataset during training. As described in [52], the DINOv2 backbone was initialized with a pretrained model, which was trained on the LVD-142M dataset.

Hardware and FPS. We trained and evaluated *WaterFormer* using an NVIDIA GeForce RTX 4090, achieving an inference speed of 1.7 FPS on this device.

Other Adaptations. Unlike the original benchmark of LaRS [86], which is a 3-class setup (water, sky and obstacles), we trained *WaterFormer* with a 4-class setup (water, sky, static obstacles, and dynamic obstacles) using panoptic segmentation labels to improve discrimination between dynamic and static obstacles. For the evaluation results, static and dynamic obstacles were merged into a single obstacle class. This decision was inspired by the observation that dynamic obstacles are usually located on the water surface.
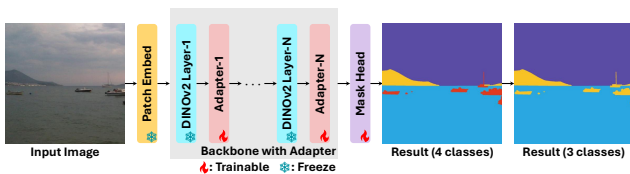

Figure 15: Brief model architecture of WaterFormer

B.2. ② WSFormer

Shanliang Yao, Runwei Guan, Xiaoyu Huang, Yi Ni
Shanliang.Yao@liverpool.ac.uk,
Runwei.Guan@liverpool.ac.uk,
x.huang42@liverpool.ac.uk,
Yi.Ni21@student.xjtlu.edu.cn,
Yancheng Institute of Technology, Hong Kong University of Science and Technology (Guangzhou), University of Liverpool, Xi'an Jiaotong-Liverpool University

Method: We designed a novel marine image semantic segmentation method, named WSFormer, inspired by Mask2Former [13]. Mask2Former utilizes masked-attention to focus on local features centered around predicted segments, thereby facilitating faster convergence and enhanced performance. Moreover, it employs multi-scale high resolution to accurately segment small regions. In developing WSFormer, we adopted the Swin-L architecture as the backbone, offering a robust and scalable framework for handling complex water scene data. Additionally, we integrated MultiHeadAttention from the Mask2Former framework, which significantly enriches feature representation and spatial awareness in our segmentation task.

Datasets: For the pretraining phase, we employed the WaterScenes dataset [79], a comprehensive collection of water-related scenes that spans a diverse array of environments and conditions. This dataset is particularly well-suited for our purposes, owing to its extensive coverage of various water scenarios accompanied by semantic segmentation annotations. Following the pretraining stage, we fine-tuned our model using the LaRS dataset [86], as specified in this challenge.

Training: We conducted our training on a NVIDIA RTX 4090 GPU, equipped with 24GB of memory. The training process was configured with a batch size of 2 to ensure efficient computation and memory utilization. For optimization, we employed the AdamW optimizer, with a learning rate of 0.0001, an epsilon value of 1e-8 to prevent division by zero, a weight decay of 0.05 for model regularization, and betas set to (0.9, 0.999) to control the exponential moving averages of the gradient and its square. To facilitate a stable and effective learning process, we implemented a warm-up strategy followed by a polynomial learning rate scheduler, spanning a total of 160,000 iterations. This scheduling approach allowed for a gradual increase in the learning rate at the outset, followed by a smooth decay, thereby enhancing the model's convergence and performance. To enhance the robustness and generalization of our model, we employed a suite of data augmentation techniques, including RandomResize, RandomCrop, RandomFlip, and PhotoMetricDistortion. Additionally, we integrated three loss functions—classification loss, mask loss, and dice loss—to comprehensively measure the discrepancy between predicted and true class labels, ensure accurate segmentation mask prediction, and optimize the model's performance for

both classification and segmentation tasks.

Inference: We utilized the same device for inference as for training. Additionally, we implemented Test Time Augmentation (TTA), a sophisticated data augmentation strategy tailored specifically for the testing phase. By aggregating predictions from each augmented version of the image, we generated a more precise and reliable final prediction, thereby enhancing the overall accuracy and robustness of our model's performance.

Results: We achieved the 2nd place in the MaCVi 2025 challenge. Our WSFormer model receives an evaluated Quality (Q) value of 79.8, which is a composite metric that integrates general segmentation quality, as measured by the mIoU, and detection quality, as assessed by the F1 score.

B.3. ③ Advanced K-Net

Himanshu Kumar
himanshu9082@gmail.com
Independent Researcher

All of my submissions are marked with Individual as an author in the leaderboard. I have used the K-Net: Towards Unified Image Segmentation method provided in the mmsegmentation-macvi repo.
I have experimented with different Swin transformer backbones, particularly Swin tiny and large. Swin Tiny is trained on the ImageNet-1K dataset. Swin large is pre-trained on a large dataset, ImageNet-22K, which can significantly improve performance on smaller datasets. No extra dataset was used to train the model. Swin large has two variants, with a patch size of 224 and 384. The larger patch variant performed better in terms of mIoU. To capture finer details of obstacles, I varied the image scale up to the size of 2560 x 1280. For optimization, I replaced Adam with Lion, which improves convergence and resulted in a marginal increase in mIoU. I tried introducing stochasticity to the model with a stochastic head, which did not yield significant results.
For the training pipeline, resizing, random crop and filling, normalization, photometric distribution, and padding were applied. For validation and inference, only Resize and normalization were performed.
The best-performing model in terms of Quality has $swin\_large\_patch4\_window7\_224\_22k\_20220308 - d5bdebaf.pth$ as the backbone, and images resized to 2048x1024. I have trained the model on a single Nvidia A100 GPU with a batch size of 4 for 80,000 iterations. AdamW, as an optimizer with a weight decay of 0.0005 and an initial learning rate of 6e-05, was used, and it decayed by 0.1 after 60000 and 72000 iterations. Gradient clipping and StepLR scheduler were incorporated into training. The best validation mIoU model was saved every 8000 iterations. The model took 26 hrs for training, and 2.5 images per second was the inference speed.

C. USV-based Embedded Obstacle Segmentation

C.1. ① RSOS-Net

Yuan Feng
fengyuan@dlum.edu.cn, 931772830@qq.com
Dalian Maritime University, School of Marine Engineering

Method:
Inspired by the encoder-decoder architecture, a realtime surface obstacle segmentation network (RSOS-Net) is created to enable online surface-obstacle detection for an unmanned waterborne vehicle. The network architecture primarily consists of an encoder section and a decoder section. In the encoder, we utilize ResNet-101 [28] as the backbone network to extract multi-scale features. Additionally, at the final stage of the encoder, we have designed the fast pyramid pooling module (FPPM), which effectively expands the receptive field by combining global average pooling and cascaded average pooling operations, enabling it to capture global and local feature information. It is noteworthy that the integration of local and global contextual information is crucial for distinguishing between water surface disturbances and real obstacles. The decoder comprises a lightweight FPN [43] and an attentionbased feature fusion module (AFFM). Specifically, RSOSNet utilizes a standard encoder network to generate multiresolution features, which are then seamlessly integrated into the decoder through the FPN structure. Notably, unlike the original FPN, RSOS-Net employs separable convolutions to replace the 3×3 convolutions in the original FPN and reduces the number of channels to 256, thereby achieving a lightweight FPN structure. Moreover, the AFFM module, employing a channel-spatial attention mechanism, causes RSOS-Net to focus more on real obstacles, reducing false positives and missed detections. Finally, the outputs of the lightweight FPN are fused through the AFFM and passed through an FCN segmentation head to obtain the final results.

Training:
We implemented RSOS-Net using the MMSegmentation framework with an image input size of 768×384 and a batch size of 16. The training was conducted on an NVIDIA RTX 3090 GPU equipped with 24G of memory. During the training process, SGD was employed, with a total of 160, 000 iterations conducted. In terms of data augmentation, techniques such as random flipping, cropping, brightness adjustment, and saturation modification were incorporated to enhance the diversity of the training data. As for the dataset, LaRS [86] was exclusively utilized for both the training and

validation phases. The pretrained weights of the backbone network were sourced from ImageNet-1K. Regarding the loss function, a combination of cross-entropy loss, dice loss, and focal loss was adopted, with a specific ratio of 1 : 2 : 1.

Observations:

- In the versions of RSOS-Net we submitted, the one with the ID 14161, which has a Q-score of 64.2 and an FPS of 85.1, uses ResNet-101 as its backbone network. The other version with the ID 14100, featuring a Q-score of 63.6 and an FPS of 102.8, employs ResNet-50 as its backbone. Both versions share the same training methodologies apart from the backbone networks.

- The work on RSOS-Net has been summarized into a paper and submitted for publication. If all goes well, it will be publicly available soon. The code for RSOS-Net is publicly accessible at `https://github.com/Yuan-Feng1998`.

C.2. ② Seg-aware Ensemble (EFFNet)

Yi-Ching Cheng, Tzu-Yu Lin, Chia-Ming Lee, Chih-Chung Hsu
`{annie30133, lspss97127, zuw408421476}@gmail.com, cchsu@gs.ncku.edu.tw`
ACVLab, National Cheng Kung University

Method:

We trained two models and combined them to get the final ensemble model. Inspired by the approach of last year's second-place team, we selected the lightweight network architectures and further improved prediction accuracy through the ensemble technique. The first model employs ResNet-50 as the encoder paired with DeepLabv3+ as the decoder, while the second uses ResNet-101 with DeepLabv3+. Both backbones were pretrained on ImageNet, and only the LaRS dataset was used for training.

Training:

The training configurations for the two models are outlined below:

- Device: 2 × RTX 2080 Ti / 2 × RTX 3090
- Epochs: 150 / 200
- Batch size: 16 / 32
- Learning rate: 0.0001 for both
- Loss function: Dice loss + weighted cross-entropy loss for both
- Optimizer: AdamW for both
- Scheduler: Cosine annealing for both
- Augmentations: Horizontal flip, resize / Horizontal flip, resize, color jitter, unsharp masking, affine transform, and rotation

Observations:

- We observed that extending the training duration consistently enhanced model performance, whereas additional augmentations and larger backbones did not yield significant improvements. Using ResNet-50 as the encoder with random horizontal flip augmentation resulted in strong performance, achieving a Q score of 60.8, F1-score of 63.6, and mIoU of 95.6 on the leaderboard.

- To capture more complex semantic features, we configured the encoder to output multi-scale feature maps.

- In experiments involving different encoders, we noticed substantial performance drops in some models after quantization. Selecting an encoder that aligns with the characteristics of maritime data and maintains stability post-quantization could be a promising direction for further improvement.

C.3. Baseline methods

MaCVi Organizers

We include winning methods from last year's competition eWaSR-RN50 and Mari-MobileSegNet as baseline methods.

D. USV-based Panoptic Segmentation

D.1. ① MaskDINO

Jannik Sheikh[1], Andreas Michel[1], Wolfgang Gross[1], [2]Martin Weinmann
[1]`{firstname.lastname}@iosb.fraunhofer.de`,
[2]`martin.weinmann@kit.edu`
Fraunhofer IOSB

This technical report describes our solutions to the 3rd Workshop on Maritime Computer Vision (MaCVi) USV-based Panoptic Segmentation challenge. We employed Mask DINO [40], an extension of the detection transformer model DINO [83]. By incorporating a mask prediction branch and creating a pixel embedding map derived from the backbone and transformer encoder features, the model is capable of performing various image segmentation tasks, including panoptic segmentation. We made use of the official implementation of the COCO pre-trained Mask DINO that utilizes an ImageNet-22K [16] pre-trained Swin-L [47] Vision Transformer. Our training was performed on four NVIDIA V100 32GB graphics cards. We trained Mask DINO on the LaRS [86] dataset for 45000 iterations. AdamW [49] was used as an optimizer with a learning rate of `1e-4`.

During training, the images were randomly flipped horizontally, resized at multiple scales within a defined range and cropped to 1024×1024 pixels. In addition, gradient clipping and a learning rate multiplier of 0.1 were applied to the backbone. Testing was performed on an NVIDIA V100 32GB graphics card. The inference speed was approximately one

FPS. The test pipeline consists of resizing the input image to 1242×2208 ($H \times W$). The proposed model achieves a PQ of 53.9 with an F1-Score of 76.5 on the LaRS test dataset. Further analysis of the results showed a very high PQ_{st} of 92.3 and a significant performance decline of PQ_{th} with 39.4. To address this performance gap, we investigated the potential integration of a Vision Language Model, specifically Llama 3.2 Vision [22]. Concretely, for any instance detected by Mask DINO belonging to the "things" category, we assessed whether Llama would provide the same category name as Mask DINO given the ground truth categories. By aligning the results of these two models, we aimed to improve the recognition quality (RQ) score and thus the overall quality. Although the performance (PQ of 52.1) of that combined approach did not improve the individual performance, the results showed promising trends that warrant further research.

D.2. ② PanopticWaterFormer

Seongju Lee, Junseok Lee, Kyoobin Lee
{lsj2121,junseoklee}@gm.gist.ac.kr,
kyoobinlee@gist.ac.kr
Gwangju Institute of Science and Technology (GIST)

Method. *PanopticWaterFormer* combines the inference results of WaterFormer for semantic segmentation and Cascade Mask R-CNN [7] with the InternImage (Large) [68] backbone for instance segmentation. This approach harnesses the strong segmentation capability of WaterFormer for stuff classes. The detailed model architecture of WaterFormer is described in the USV-based Semantic Segmentation section. Our implementation is based on MMDetection [9] framework.

Training Details. For training Cascade Mask R-CNN, the AdamW [50] optimizer was employed with a learning rate of 0.0001, a weight decay of 0.05, epsilon set to 10^{-8}, and betas set to (0.9, 0.999). The batch size was set to 2, and the number of training epochs was set to 24. The learning rate was adjusted at epochs 8 and 11 by multiplying it by a factor of 0.1, with updates applied at the epoch level. Additionally, the layer-wise learning rate decay was set to 0.9 to preserve the pretrained knowledge in the earlier layers. The augmentation pipeline for training includes random horizontal flipping with a probability of 50%, large-scale jittering [25] through random resizing with a scale range of (0.1, 2.0) while maintaining the aspect ratio, and random cropping to a fixed size of 1024×1024. During inference, the images were resized to a fixed size of 2048×1024.

Datasets and Pretrained Weights. We used only the LaRS [86] dataset during training. To initialize Cascade Mask R-CNN with the InternImage backbone, we used COCO-pretrained weights [42] at the start of training.

Hardware and FPS. We evaluated *PanopticWaterFormer* using an NVIDIA H100, achieving an inference speed of 1.1 FPS on this device.

Panoptic Mask Generation. First, we obtained a segmentation map from WaterFormer, which divides the scene into stuff (water, sky, and obstacle) and things (dynamic obstacles). Second, we extracted instance masks, their corresponding bounding boxes, and predicted labels from Cascade Mask R-CNN. Instances with a confidence score below 0.5 were discarded. Finally, panoptic segmentation maps were generated by assigning instance masks to the things region of the segmentation map in descending order of size, from largest to smallest, if their bounding boxes overlapped with the things region.

D.3. ③ FC-CLIP-LaRS

Josip Šarić
josip.saric@fri.uni-lj.si
University of Ljubljana

Our submission builds upon the panoptic mask transformer FC-CLIP [81]. FC-CLIP incorporates a language-based classifier, which enables open-vocabulary recognition [56]. Specifically, the classification scores are derived from similarities between the predicted mask embeddings and the embeddings generated by a frozen CLIP [56] text encoder applied to class descriptions. To enhance the recognition of unseen classes, the scores are ensembled with zero-shot classification of mask-pooled features [26, 81] from frozen convolutional CLIP visual encoder [56]. Note that the same module serves as an image feature extractor for mask decoder. Concretely, we rely on ConvNext-L [48] backbone initalized with OpenCLIP weights [14] pretrained on the LAION dataset [61].

Our preliminary study showed that a pretrained COCO [42] FC-CLIP results in a poor performance (18.2 PQ and 50.1 mIoU) on the LaRS validation set [86]. We hypothesize this is due to a significant domain shift between COCO and LaRS. We also noticed that the default LaRS class text descriptions are short and vague, which could affect the performance of the language-based classifier. To test this hypothesis, we extended the class descriptions with additional synonyms or hyponyms (e.g. *static-obstacle* with *building*, *terrain*, *vegetation*, etc.). This lead to substantial performance boost (27.6 PQ and 91.6 mIoU).

Finally, we fine-tuned the COCO model on LaRS train for 90k iterations with batch size 8 and base learning rate 10^{-4}. We set the crop size to 512×1024 pixels, and applied random color and scale jitter. During evaluation we resize

the larger side to 2048 pixels, while maintaining the original aspect ratio. The fine-tuned model achieves 53.6 PQ and 94.9 mIoU on the LaRS validation set. On the test set, the model achieved 49.7 PQ, securing the third place in the official MaCVi Panoptic Segmentation Challenge.

It is important to note that the results of the fine-tuned model do not reflect its open-vocabulary capabilities, as the training and testing vocabularies are identical. In future work, we aim to explore open-vocabulary panoptic segmentation specifically for the maritime domain.

D.4. Baseline and PanSR

MaCVi Organizers

As the baseline, we train the Mask2Former [13] with the Swin-B backbone using MMSegmentation [15] framework with a training configuration adapted for LaRS [86]. Furthermore, we also submitted our novel PanSR method [85] to the leaderboard. PanSR introduces a new approach to query proposal generation and rethinks the training methodology for better synergy with the proposal-based queries. This leads to more robust detection of small objects and state-of-the-art performance on LaRS. More details are available in [85].

E. Underwater Image Restoration

E.1. ① Team NJUST-KMG

Yipeng LIN[1], Xiang yang[1], Nan Jiang[2], Yang Yang[1]
2396599652@qq.com, maybe_1221@163.com,
1306550598@qq.com, yyang@njust.edu.cn
[1]*Nanjing University of Science and Technology*
[2]*Nanjing University*

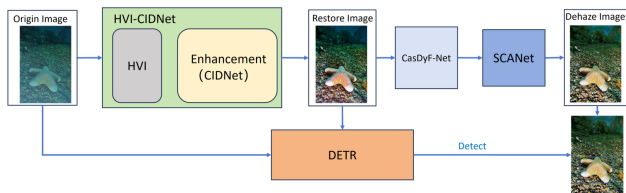The overall framework of our method is illustrated in

Figure 16: Overview of the architecture proposed by Team NJUST-KMG for underwater image restoration and marine species detection.

Figure 16. The challenge is divided into two parts: image restoration and object detection. Due to the lack of an end-to-end model framework, we trained separate models for these two parts. For the image restoration task, we adopted a two-stage approach. Since the dataset primarily consists of large images, we used the efficient image restoration method HVI-CIDNet [73] in the first stage. In the second stage, we employed the image dehazing methods CasDyF-Net [80]

and SCANet [27]. For object detection, we used the DETR [8] model. With the rapid development of deep learning, many powerful deep learning models [66, 72, 77], have emerged. We experimented with several image restoration models, including U-shape [53], UDAformer [62], and the solution from team SYSU-FVL-T2 for the NTIRE 2024 Low Light Enhancement Challenge [45]. However, we found that due to the large images in the RSUIGM [18] dataset, these models performed poorly during training. Therefore, we used HVICIDNet, an efficient and outstanding image restoration network. However, upon observing the restored images, we noticed large areas with shallow color overlays that resembled artificially generated fog. Therefore, after the first stage, we restored the training dataset and used them to train dehaze models CasDyF-Net and SCANet. The restored images were first processed by the fine-tuned CasDyF-Net and then by the pre-trained SCANet. For the object detection task, we used DETR as our main model and adopted a two-stage fine-tuning strategy. The model was trained on the original dataset and then fine-tuned on the dataset with initially restored images. In order to mitigate the impact of the long-tail distribution, we applied weight allocation to the classification head. Finally, we achieved the following results: for image restoration, CCF: 0.077, UCIQE: 0.571, and UIQM: 0.7; and for object detection, mAP: 0.125, F1: 0.125, and mIoU: 0.693. And our model can process two large images similar size to test dataset per second on an RTX 3090.

E.1.1 Training Details

Dataset. We only used the official RSUIGM dataset for training. Additionally, the pre-trained models HVI-CIDNet, CasDyF-Net, SCANet and DETR are pretrained on the LOLV1 [70], Haze4K [46], NTIRE and ImageNet [58], respectively.

Method	mAP	F1	mIoU	CCF	UCIQE	UIQM
baseline	0	0	0.00	0.04	0.498	0.193
HVI-CIDNet+DETR	0.093	0.093	0.691	0.038	0.547	0.493
HVI-CIDNet+DETR(LT)	**0.143**	**0.143**	**0.636**	0.038	0.547	0.493
HVI-CIDNet+CasDyF-Net+DETR(LT)	0.090	0.090	0.561	0.032	0.530	0.696
HVI-CIDNet+CasDyF-Net+SCA-Net+DETR(LT)	0.125	0.125	0.693	0.077	**0.571**	**0.700**

Table 6: Performance comparison of different methods

Implementation Details. We are training models on a single RTX 3090. During the training process, the dataset is split into a training set and validation set by 9:1. For HVI-CIDNet, the training strategy from MIRNet-v2 [69] is adopted, where images are progressively trained at sizes of 256/512/1024 for 30/30/10 epochs, respectively, and save the highest PSNR model. For CasDyF-Net, the repaired dataset is used for 10 epochs of training. For DETR, we fine-tuned the pre-trained DETR model (with a ResNet50 backbone) for 200 epochs on the initial dataset, and then fine-tuned

it for 50 epochs on the restored images. The experimental results are shown in the Table 6.

E.2. ② Team BUPT MCPRL

Yutang Lu, Fei Feng
luyutang8610@163.com,
wusaqi09@gmail.com
Beijing University of Posts and Telecommunications, Beijing, China

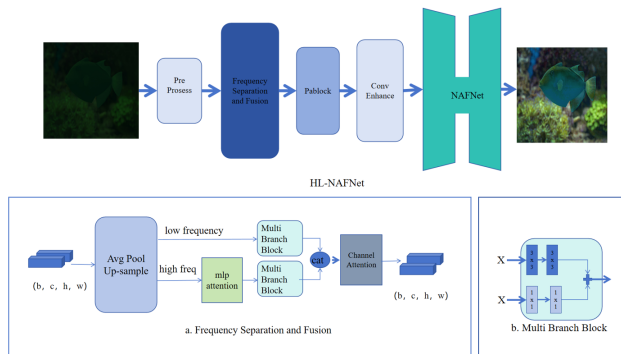To enhance the visual quality of underwater images, we

Figure 17: Overview of the architecture proposed by Team BUPT MCPRL for underwater image restoration and marine species detection.

have proposed the HL-NAFNet model, which integrates frequency separation and fusion technology with NAFNet [10] post-processing. This allows the image to undergo an initial restoration phase, followed by a second phase of NAFNet restoration, aiming to enhance the clarity and color fidelity of the image. The model architecture, as shown in Figure 17, consists of the following key modules:

Frequency Separation and Fusion: After convolutional pre-processing, we reduce the spatial dimensions of the image through average pooling to extract low-frequency information. High-frequency information is obtained by subtracting the upsampled low-frequency information from the original image. For the high-frequency information, we use Multi-Layer Perceptron Attention to highlight image details. The low and high-frequency feature images are then processed in parallel through a multi-branch block to enhance the expression of features. Finally, channel attention is used to fuse low and high-frequency information, enhancing the final output.

PABlock (Pixel Attention Block): Utilizing Global Average Pooling, this block captures a comprehensive statistical profile of the feature map. It then utilizes 1x1 convolutions with a ReLU activation to craft an attention map.

Training Details. Adopting AdamW optimizer with $\beta_1 = 0.9$ and $\beta_2 = 0.999$ for training 100epochs. The initial learning rate was set to 10^{-4}. The cosine annealing strategy

is employed to decrease the learning rates to 10^{-6} . All experiments are conducted on two NVIDIA GeForce RTX 4090 24GB GPUs.in the NAFnet the enc_blks is $[2, 2, 4, 8]$, the middle_blk_num is 12 and the dec_blks is $[2, 2, 2, 2]$.

E.2.1 detect and classify

Detecting the restored underwater images based on YOLOv5s [30].The data set uses the original underwater images in RSUIGM to filter the original images according to the requirements of target detection and input training. The experimental platform environment is Linux system with Tesla T4 graphics card. The input size is $(1080, 1080)$, the batchsize is 32, the initial learning rate is 0.01, the SGD optimizer is used, and the epoch is 100.

E.3. ③ Team MTU

Ali Awad[1], Evan Lucas[2], Ashraf Saleem[1]
aawad@mtu.edu, eglucas@mtu.edu,
ashraf@mtu.edu
[1]*Department of Applied Computing, College of Computing, Michigan Technological University, Houghton, MI 49931, USA*
[2]*Institute of Computing and Cybersystems, Michigan Technological University, Houghton, MI 49931, USA*

Our team used the Texture Enhancement Model Based on Blurriness and Color Fusion (TEBCF) method [82] based on extensive benchmarking studies that consider the impact of image enhancement on detection in underwater conditions [3, 59] using publicly available object detection datasets, including one made by our group [23, 60]. TEBCF uses multi-scale fusion to combine the outputs of two input pipelines, one that uses the RGB color space to improve sharpness through a dehazing based on a dark channel prior, and another, and another that uses CIELAB space for color correction and brightness adjustment. Since TEBCF is a non-data-driven method, it requires no training and can be used directly for inference on a CPU. The default parameters of TEBCF provided by the authors are used in this work without any modification. We ran TEBCF on a Xeon W-2295 CPU in parallel mode with 18 workers resulting in approximately 4 images per minute. On the detection side, we used the SuperGradients [2] library to implement YOLO-NAS detection model on a Linux server with two Nvidia Tesla V100 GPUs. The training was performed with a batch size of 16, AdamW optimizer, decay of 0.00001, large YOLO architecture, and COCO pre-trained weights. Separate detection models of YOLO-NAS are trained on original and enhanced images. Our findings reveal that image enhancement has the potential to improve object detection in some cases despite its negative overall performance on detection. In addition, we noticed that the current Image Quality Metrics (IQM) are very sensitive and

do not accurately represent human perception. For example, TEBCF outperforms many state-of-the-art enhancement models by a large margin in terms of IQM, yet it produces very noisy and reddish images compared to other models. Finally, we noticed that enhancement could help in revealing hidden objects that are missed by human annotators resulting in inaccurate dataset annotations and unreliable results.

E.4. Team ACVLab

Ching-Heng Cheng, Yu-Fan Lin, Tzu-Yu Lin, Chih-Chung Hsu[*]
henry918888@gmail.com,
aas12as12as12tw@gmail.com,
lspss97127@gmail.com,
cchsu@gs.ncku.edu.tw
ACVLab, National Cheng Kung University
[*]*corresponding author*

E.4.1 Description

We trained two models to perform inference sequentially to obtain the final result. Drawing inspiration from the color space fusion approach, which is commonly used in UIE tasks, as well as from the attention mechanisms prevalent in natural image restoration (IR), we selected TCTL-Net [41], a network structure based on the LAB color space, as our baseline model. We further modified the original architecture based on our expertise to enhance the restoration quality. Additionally, we added an MLP head to predict the downwelling depth (d) and the attenuation coefficient (k) of a degraded image. However, the large size of the input image presents a significant challenge to general models, particularly those that rely on global feature extraction. These models are not well-suited for slicing the image into patches to reduce memory usage. To address this, we trained a lightweight fusion model that combines the degraded original-size image with the restored small-size image, resulting in a full-size restored output. Both models were trained using only the provided RSUIGM dataset [18]. For the detection component, we utilized Grounding DINO [83] with pre-trained weights as the detector and fine-tuned the threshold settings to achieve improved results.

E.4.2 Training Details

The training configurations for the two models are outlined below:

- Device: 2 × RTX 2080 Ti / 1 × RTX 2080 Ti

- Epochs: 100 / 50

- Batch size: 24 / 1

- Learning rate: 0.0001 for both

- Loss function: L1 loss + L2 loss + SSIM loss/ L1 loss + L2 loss

- Optimizer: AdamW for both

- Scheduler: Cosine annealing for both

- Augmentations: Horizontal flip for both

- Inference time: 266ms per image on a 2080Ti GPU

E.4.3 Observations

We observed that synthetic degraded images with high levels of depth or attenuation may introduce artifacts between aquatic animals and the background. These synthetic degraded images appear unnatural, which causes the restoration results to be dependent on the specific degradation conditions. Furthermore, since the evaluation metrics are non-reference based and our training strategy is based on supervision, the results may not fully capture a rich color representation. This is because the ground truth images may not always be as colorful. This insufficiency represents an area that deserves attention and improvement in our future work.

References

[1] Segmentation Models (PyTorch) Repository. https://github.com/qubvel/segmentation_models.pytorch. Accessed: 2022-11-09.

[2] Shay Aharon, Louis-Dupont, Ofri Masad, Kate Yurkova, Lotem Fridman, Lkdci, Eugene Khvedchenya, Ran Rubin, Natan Bagrov, Borys Tymchenko, Tomer Keren, Alexander Zhilko, and Eran-Deci. Super-gradients, 2021.

[3] Ali Awad, Ashraf Saleem, Sidike Paheding, Evan Lucas, Serein Al-Ratrout, and Timothy C. Havens. Evaluating the impact of underwater image enhancement on object detection performance: A comprehensive study, 2024.

[4] Domenico Bloisi. Background modeling and foreground detection for maritime video surveillance. *Chapter in Handbook on Background Modeling and Foreground Detection for Video Surveillance: Traditional and Recent Approaches, Implementations, Benchmarking and Evaluation, Chapman and Hall/CRC*, pages 14–1, 2014.

[5] Borja Bovcon and Matej Kristan. WaSR–A Water Segmentation and Refinement Maritime Obstacle Detection Network. *IEEE Transactions on Cybernetics*, pages 1–14, 2021.

[6] Borja Bovcon, Jon Muhovič, Janez Perš, and Matej Kristan. The mastr1325 dataset for training deep usv obstacle detection models. In *Int. Conf. Intell. Robots and Systems*, pages 3431–3438. IEEE, 2019.

[7] Zhaowei Cai and Nuno Vasconcelos. Cascade r-cnn: high quality object detection and instance segmentation. *IEEE transactions on pattern analysis and machine intelligence*, 43(5):1483–1498, 2019.

[8] Nicolas Carion, Francisco Massa, Gabriel Synnaeve, Nicolas Usunier, Alexander Kirillov, and Sergey Zagoruyko. End-to-end object detection with transformers. In *European conference on computer vision*, pages 213–229. Springer, 2020.

[9] Kai Chen, Jiaqi Wang, Jiangmiao Pang, Yuhang Cao, Yu Xiong, Xiaoxiao Li, Shuyang Sun, Wansen Feng, Ziwei Liu, Jiarui Xu, et al. Mmdetection: Open mmlab detection toolbox and benchmark. *arXiv preprint arXiv:1906.07155*, 2019.

[10] Liangyu Chen, Xiaojie Chu, Xiangyu Zhang, and Jian Sun. Simple baselines for image restoration. *arXiv preprint arXiv:2204.04676*, 2022.

[11] Liang-Chieh Chen, George Papandreou, Iasonas Kokkinos, Kevin Murphy, and Alan L. Yuille. Deeplab: Semantic image segmentation with deep convolutional nets, atrous convolution, and fully connected crfs. *IEEE Transactions on Pattern Analysis and Machine Intelligence*, 40(4):834–848, 2018.

[12] Xiangning Chen, Chen Liang, Da Huang, Esteban Real, Kaiyuan Wang, Hieu Pham, Xuanyi Dong, Thang Luong, Cho-Jui Hsieh, Yifeng Lu, et al. Symbolic discovery of optimization algorithms. *Advances in neural information processing systems*, 36, 2024.

[13] Bowen Cheng, Ishan Misra, Alexander G. Schwing, Alexander Kirillov, and Rohit Girdhar. Masked-attention mask transformer for universal image segmentation. 2022.

[14] Mehdi Cherti, Romain Beaumont, Ross Wightman, Mitchell Wortsman, Gabriel Ilharco, Cade Gordon, Christoph Schuhmann, Ludwig Schmidt, and Jenia Jitsev. Reproducible scaling laws for contrastive language-image learning. In *Proceedings of the IEEE/CVF Conference on Computer Vision and Pattern Recognition*, pages 2818–2829, 2023.

[15] MMSegmentation Contributors. MMSegmentation: Openmmlab semantic segmentation toolbox and benchmark. `https://github.com/open-mmlab/mmsegmentation`, 2020.

[16] Jia Deng, Wei Dong, Richard Socher, Li-Jia Li, Kai Li, and Li Fei-Fei. Imagenet: A large-scale hierarchical image database. In *2009 IEEE conference on computer vision and pattern recognition*, pages 248–255. Ieee, 2009.

[17] Chaitra Desai, Nikhil Akalwadi, Amogh Joshi, Sampada Malagi, Chinmayee Mandi, Ramesh Ashok Tabib, Ujwala Patil, and Uma Mudenagudi. Lightnet: Generative model for enhancement of low-light images. In *Proceedings of the IEEE/CVF International Conference on Computer Vision (ICCV) Workshops*, pages 2231–2240, October 2023.

[18] Chaitra Desai, Sujay Benur, Ujwala Patil, and Uma Mudenagudi. Rsuigm: Realistic synthetic underwater image generation with image formation model. *ACM Trans. Multimedia Comput. Commun. Appl.*, 21(1), Dec. 2024.

[19] Chaitra Desai, Sujay Benur, Ramesh Ashok Tabib, Ujwala Patil, and Uma Mudenagudi. Depthcue: Restoration of underwater images using monocular depth as a clue. In *Proceedings of the IEEE/CVF Winter Conference on Applications of Computer Vision (WACV) Workshops*, pages 196–205, January 2023.

[20] Chaitra Desai, Badduri Sai Sudheer Reddy, Ramesh Ashok Tabib, Ujwala Patil, and Uma Mudenagudi. Aquagan: Restoration of underwater images. In *Proceedings of the IEEE/CVF Conference on Computer Vision and Pattern Recognition (CVPR) Workshops*, pages 296–304, June 2022.

[21] Chaitra Desai, Ramesh Ashok Tabib, Sai Sudheer Reddy, Ujwala Patil, and Uma Mudenagudi. Ruig: Realistic underwater image generation towards restoration. In *Proceedings of the IEEE/CVF Conference on Computer Vision and Pattern Recognition (CVPR) Workshops*, pages 2181–2189, June 2021.

[22] Aaron Grattafiori et al. The llama 3 herd of models, 2024.

[23] Chenping Fu, Risheng Liu, Xin Fan, Puyang Chen, Hao Fu, Wanqi Yuan, Ming Zhu, and Zhongxuan Luo. Rethinking general underwater object detection: Datasets, challenges, and solutions. *Neurocomputing*, 517:243–256, 2023.

[24] Antonio-Javier Gallego, Antonio Pertusa, Pablo Gil, and Robert B Fisher. Detection of bodies in maritime rescue operations using unmanned aerial vehicles with multispectral cameras. *Journal of Field Robotics*, 36(4):782–796, 2019.

[25] Golnaz Ghiasi, Yin Cui, Aravind Srinivas, Rui Qian, Tsung-Yi Lin, Ekin D Cubuk, Quoc V Le, and Barret Zoph. Simple copy-paste is a strong data augmentation method for instance segmentation. In *Proceedings of the IEEE/CVF conference on computer vision and pattern recognition*, pages 2918–2928, 2021.

[26] Golnaz Ghiasi, Xiuye Gu, Yin Cui, and Tsung-Yi Lin. Scaling open-vocabulary image segmentation with image-level labels. In *European Conference on Computer Vision*, pages 540–557. Springer, 2022.

[27] Yu Guo, Yuan Gao, Wen Liu, Yuxu Lu, Jingxiang Qu, Shengfeng He, and Wenqi Ren. Scanet: Self-paced semi-curricular attention network for non-homogeneous image dehazing. In *Proceedings of the IEEE/CVF Conference on Computer Vision and Pattern Recognition*, pages 1885–1894, 2023.

[28] Kaiming He, Xiangyu Zhang, Shaoqing Ren, and Jian Sun. Deep residual learning for image recognition. In *Proceedings of the IEEE conference on computer vision and pattern recognition*, pages 770–778, 2016.

[29] Dan Hendrycks and Kevin Gimpel. Gaussian error linear units (gelus). *arXiv preprint arXiv:1606.08415*, 2016.

[30] Glenn Jocher, Ayush Chaurasia, and Jing Qiu. Ultralytics YOLO, Jan. 2023.

[31] Urška Kanjir, Harm Greidanus, and Krištof Oštir. Vessel detection and classification from spaceborne optical images: A literature survey. *Remote sensing of environment*, 207:1–26, 2018.

[32] Benjamin Kiefer, Matej Kristan, Janez Perš, Lojze Žust, Fabio Poiesi, Fabio Andrade, Alexandre Bernardino, Matthew Dawkins, Jenni Raitoharju, Yitong Quan, Adem Atmaca, Timon Höfer, Qiming Zhang, Yufei Xu, Jing Zhang, Dacheng Tao, Lars Sommer, Raphael Spraul, Hangyue Zhao, Hongpu Zhang, Yanyun Zhao, Jan Lukas Augustin, Eui-ik Jeon, Impyeong Lee, Luca Zedda, Andrea Loddo, Cecilia Di Ruberto, Sagar Verma, Siddharth Gupta, Shishir Muralidhara, Niharika Hegde, Daitao Xing, Nikolaos Evangeliou, Anthony Tzes, Vojtěch Bartl, Jakub Špaňhel, Adam Herout, Neelanjan Bhowmik, Toby P. Breckon, Shivanand Kundargi, Tejas Anvekar, Ramesh Ashok Tabib, Uma Mudenagudi, Arpita Vats,

Yang Song, Delong Liu, Yonglin Li, Shuman Li, Chenhao Tan, Long Lan, Vladimir Somers, Christophe De Vleeschouwer, Alexandre Alahi, Hsiang-Wei Huang, Cheng-Yen Yang, Jenq-Neng Hwang, Pyong-Kun Kim, Kwangju Kim, Kyoungoh Lee, Shuai Jiang, Haiwen Li, Zheng Ziqiang, Tuan-Anh Vu, Hai Nguyen-Truong, Sai-Kit Yeung, Zhuang Jia, Sophia Yang, Chih-Chung Hsu, Xiu-Yu Hou, Yu-An Jhang, Simon Yang, and Mau-Tsuen Yang. 1st workshop on maritime computer vision (macvi) 2023: Challenge results. In *Proceedings of the IEEE/CVF Winter Conference on Applications of Computer Vision (WACV) Workshops*, pages 265–302, January 2023.

[33] Benjamin Kiefer, David Ott, and Andreas Zell. Leveraging synthetic data in object detection on unmanned aerial vehicles. *arXiv preprint arXiv:2112.12252*, 2021.

[34] Benjamin Kiefer, Yitong Quan, and Andreas Zell. Approximate supervised object distance estimation on unmanned surface vehicles, 2025.

[35] Benjamin Kiefer, Lojze Žust, Matej Kristan, Janez Perš, Matija Teršek, Arnold Wiliem, Martin Messmer, Cheng-Yen Yang, Hsiang-Wei Huang, Zhongyu Jiang, Heng-Cheng Kuo, Jie Mei, Jenq-Neng Hwang, Daniel Stadler, Lars Sommer, Kaer Huang, Aiguo Zheng, Weitu Chong, Kanokphan Lertniphonphan, Jun Xie, Feng Chen, Jian Li, Zhepeng Wang, Luca Zedda, Andrea Loddo, Cecilia Di Ruberto, Tuan-Anh Vu, Hai Nguyen-Truong, Tan-Sang Ha, Quan-Dung Pham, Sai-Kit Yeung, Yuan Feng, Nguyen Thanh Thien, Lixin Tian, Andreas Michel, Wolfgang Gross, Martin Weinmann, Borja Carrillo-Perez, Alexander Klein, Antje Alex, Edgardo Solano-Carrillo, Yannik Steiniger, Angel Bueno Rodriguez, Sheng-Yao Kuan, Yuan-Hao Ho, Felix Sattler, Matej Fabijanić, Magdalena Šimunec, and Nadir Kapetanović. 2nd workshop on maritime computer vision (macvi) 2024: Challenge results. In *Proceedings of the IEEE/CVF Winter Conference on Applications of Computer Vision (WACV) Workshops*, pages 869–891, January 2024.

[36] Benjamin Kiefer and Lojze Žust. Macvi website. `https://macvi.org/`. Accessed: 2025-01-14.

[37] Alexander Kirillov, Kaiming He, Ross Girshick, Carsten Rother, and Piotr Dollar. Panoptic segmentation. In *Proceedings of the IEEE Computer Society Conference on Computer Vision and Pattern Recognition*, volume 2019-June, pages 9396–9405. IEEE Computer Society, June 2019.

[38] Matej Kristan, Jiri Matas, Aleš Leonardis, Tomas Vojíř, Roman Pflugfelder, Gustavo Fernández, Georg Nebehay, Fatih Porikli, and Luka Čehovin. A novel performance evaluation methodology for single-target trackers. *IEEE Transactions on Pattern Analysis and Machine Intelligence*, 38(11):2137–2155, 2016.

[39] Mykola Lavreniuk. Spidepth: Strengthened pose information for self-supervised monocular depth estimation, 2024.

[40] Feng Li, Hao Zhang, Huaizhe xu, Shilong Liu, Lei Zhang, Lionel M. Ni, and Heung-Yeung Shum. Mask DINO: Towards A Unified Transformer-based Framework for Object Detection and Segmentation, Dec. 2022.

[41] Kunqian Li, Hongtao Fan, Qi Qi, Chi Yan, Kun Sun, and QM Jonathan Wu. Tctl-net: Template-free color transfer learning for self-attention driven underwater image enhance-ment. *IEEE Transactions on Circuits and Systems for Video Technology*, 2023.

[42] T. Lin, M. Maire, S. Belongie, J. Hays, P. Perona, D. Ramanan, P. Dollár, and C. L. Zitnick. Microsoft coco: Common objects in context. In *Eur. Conf. Comput. Vis.*, pages 740–755, 2014.

[43] Tsung-Yi Lin, Piotr Dollár, Ross Girshick, Kaiming He, Bharath Hariharan, and Serge Belongie. Feature pyramid networks for object detection. In *Proceedings of the IEEE conference on computer vision and pattern recognition*, pages 2117–2125, 2017.

[44] Shaohua Liu, Yuchong Yang, Xingjian Jing, Bin Li, Hao Liu, Zhu Shangwei, and Chundong She. *BiFormer: An End-to-End Deep Learning Approach for Enhanced Image-Based Photoplethysmography and Heart Rate Accuracy*. 01 2024.

[45] Xiaoning Liu, Zongwei Wu, Ao Li, Florin-Alexandru Vasluianu, Yulun Zhang, Shuhang Gu, Le Zhang, Ce Zhu, Radu Timofte, Zhi Jin, et al. Ntire 2024 challenge on low light image enhancement: Methods and results. *arXiv preprint arXiv:2404.14248*, 2024.

[46] Ye Liu, Lei Zhu, Shunda Pei, Huazhu Fu, Jing Qin, Qing Zhang, Liang Wan, and Wei Feng. From synthetic to real: Image dehazing collaborating with unlabeled real data. In *Proceedings of the 29th ACM international conference on multimedia*, pages 50–58, 2021.

[47] Ze Liu, Yutong Lin, Yue Cao, Han Hu, Yixuan Wei, Zheng Zhang, Stephen Lin, and Baining Guo. Swin transformer: Hierarchical vision transformer using shifted windows. In *Proceedings of the IEEE/CVF International Conference on Computer Vision*, pages 10012–10022, 2021.

[48] Zhuang Liu, Hanzi Mao, Chao-Yuan Wu, Christoph Feichtenhofer, Trevor Darrell, and Saining Xie. A convnet for the 2020s. In *Proceedings of the IEEE/CVF conference on computer vision and pattern recognition*, pages 11976–11986, 2022.

[49] Ilya Loshchilov and Frank Hutter. Decoupled weight decay regularization. In *International Conference on Learning Representations*, 2019.

[50] Ilya Loshchilov, Frank Hutter, et al. Fixing weight decay regularization in adam. *arXiv preprint arXiv:1711.05101*, 5, 2017.

[51] Armin Masoumian, Hatem A. Rashwan, Julián Cristiano, M. Salman Asif, and Domenec Puig. Monocular depth estimation using deep learning: A review. *Sensors*, 22(14), 2022.

[52] Maxime Oquab, Timothée Darcet, Théo Moutakanni, Huy V Vo, Marc Szafraniec, Vasil Khalidov, Pierre Fernandez, Daniel HAZIZA, Francisco Massa, Alaaeldin El-Nouby, et al. Dinov2: Learning robust visual features without supervision. *Transactions on Machine Learning Research*.

[53] Lintao Peng, Chunli Zhu, and Liheng Bian. U-shape transformer for underwater image enhancement. *IEEE Transactions on Image Processing*, 32:3066–3079, 2023.

[54] Dilip K Prasad, Huixu Dong, Deepu Rajan, and Chai Quek. Are object detection assessment criteria ready for maritime computer vision? *IEEE Transactions on Intelligent Transportation Systems*, 21(12):5295–5304, 2019.

[55] Inc. Qualcomm Technologies. Snapdragon neural processing engine (snpe), 2025. Accessed: 2025-01-02.

[56] Alec Radford, Jong Wook Kim, Chris Hallacy, Aditya Ramesh, Gabriel Goh, Sandhini Agarwal, Girish Sastry, Amanda Askell, Pamela Mishkin, Jack Clark, et al. Learning transferable visual models from natural language supervision. In *International conference on machine learning*, pages 8748–8763. PMLR, 2021.

[57] René Ranftl, Katrin Lasinger, David Hafner, Konrad Schindler, and Vladlen Koltun. Towards robust monocular depth estimation: Mixing datasets for zero-shot cross-dataset transfer, 2020.

[58] Olga Russakovsky, Jia Deng, Hao Su, Jonathan Krause, Sanjeev Satheesh, Sean Ma, Zhiheng Huang, Andrej Karpathy, Aditya Khosla, Michael Bernstein, et al. Imagenet large scale visual recognition challenge. *International journal of computer vision*, 115:211–252, 2015.

[59] Ashraf Saleem, Ali Awad, Sidike Paheding, Evan Lucas, Timothy C Havens, and Peter C Esselman. Understanding the influence of image enhancement on underwater object detection: A quantitative and qualitative study. *Remote Sensing*, 17(2):185, 2025.

[60] Ashraf Saleem, Ali Awad, Sidike Paheding, and Amy Marcarelli. Multi-class plant type detection in great lakes region using remotely operated vehicle and deep learning. In *Pattern Recognition and Tracking XXXIV*, volume 12527, pages 34–40. SPIE, 2023.

[61] Christoph Schuhmann, Romain Beaumont, Richard Vencu, Cade Gordon, Ross Wightman, Mehdi Cherti, Theo Coombes, Aarush Katta, Clayton Mullis, Mitchell Wortsman, et al. Laion-5b: An open large-scale dataset for training next generation image-text models. *Advances in Neural Information Processing Systems*, 35:25278–25294, 2022.

[62] Zhen Shen, Haiyong Xu, Ting Luo, Yang Song, and Zhouyan He. Udaformer: Underwater image enhancement based on dual attention transformer. *Computers & Graphics*, 111:77–88, 2023.

[63] Matija Teršek, Lojze Žust, and Matej Kristan. ewasr—an embedded-compute-ready maritime obstacle detection network. *Sensors*, 23(12):5386, 2023.

[64] Marek Vajgl, Petr Hurtik, and Tomáš Nejezchleba. Dist-YOLO: Fast Object Detection with Distance Estimation. *Applied Sciences*, 12(3):1354, Jan. 2022.

[65] Leon Amadeus Varga, Benjamin Kiefer, Martin Messmer, and Andreas Zell. Seadronessee: A maritime benchmark for detecting humans in open water. In *Proceedings of the IEEE/CVF Winter Conference on Applications of Computer Vision*, pages 2260–2270, 2022.

[66] Fengqiang Wan, Xiangyu Wu, Zhihao Guan, and Yang Yang. Covlr: Coordinating cross-modal consistency and intra-modal relations for vision-language retrieval. In *2024 IEEE International Conference on Multimedia and Expo (ICME)*, pages 1–6. IEEE, 2024.

[67] Chien-Yao Wang, Alexey Bochkovskiy, and Hong-Yuan Mark Liao. YOLOv7: Trainable bag-of-freebies sets new state-of-the-art for real-time object detectors. *arXiv preprint arXiv:2207.02696*, 2022.

[68] Wenhai Wang, Jifeng Dai, Zhe Chen, Zhenhang Huang, Zhiqi Li, Xizhou Zhu, Xiaowei Hu, Tong Lu, Lewei Lu, Hongsheng Li, et al. Internimage: Exploring large-scale vision foundation models with deformable convolutions. In *Proceedings of the IEEE/CVF conference on computer vision and pattern recognition*, pages 14408–14419, 2023.

[69] Syed Waqas Zamir, Aditya Arora, Salman Khan, Munawar Hayat, Fahad Shahbaz Khan, Ming-Hsuan Yang, and Ling Shao. Learning enriched features for fast image restoration and enhancement. *arXiv e-prints*, pages arXiv–2205, 2022.

[70] Chen Wei, Wenjing Wang, Wenhan Yang, and Jiaying Liu. Deep retinex decomposition for low-light enhancement. *arXiv preprint arXiv:1808.04560*, 2018.

[71] Yuwen Xiong, Zhiqi Li, Yuntao Chen, Feng Wang, Xizhou Zhu, Jiapeng Luo, Wenhai Wang, Tong Lu, Hongsheng Li, Yu Qiao, et al. Efficient deformable convnets: Rethinking dynamic and sparse operator for vision applications. In *Proceedings of the IEEE/CVF Conference on Computer Vision and Pattern Recognition*, pages 5652–5661, 2024.

[72] Haonan Xu and Yang Yang. Itp: Instance-aware test pruning for out-of-distribution detection. *arXiv preprint arXiv:2412.12566*, 2024.

[73] Qingsen Yan, Yixu Feng, Cheng Zhang, Pei Wang, Peng Wu, Wei Dong, Jinqiu Sun, and Yanning Zhang. You only need one color space: An efficient network for low-light image enhancement. *arXiv preprint arXiv:2402.05809*, 2024.

[74] Lingxiao Yang, Ru-Yuan Zhang, Lida Li, and Xiaohua Xie. Simam: A simple, parameter-free attention module for convolutional neural networks. In Marina Meila and Tong Zhang, editors, *Proceedings of the 38th International Conference on Machine Learning*, volume 139 of *Proceedings of Machine Learning Research*, pages 11863–11874. PMLR, 18–24 Jul 2021.

[75] Yang Yang, Yurui Huang, Weili Guo, Baohua Xu, and Dingyin Xia. Towards global video scene segmentation with context-aware transformer. *Proceedings of the AAAI Conference on Artificial Intelligence*, 37(3):3206–3213, Jun. 2023.

[76] Yang Yang, Hongpeng Pan, Qing-Yuan Jiang, Yi Xu, and Jinghui Tang. Learning to rebalance multi-modal optimization by adaptively masking subnetworks, 2024.

[77] Yang Yang, Fengqiang Wan, Qing-Yuan Jiang, and Yi Xu. Facilitating multimodal classification via dynamically learning modality gap. In *The Thirty-eighth Annual Conference on Neural Information Processing Systems*, 2024.

[78] Yang Yang, Jingshuai Zhang, Fan Gao, Xiaoru Gao, and Hengshu Zhu. Domfn: A divergence-oriented multi-modal fusion network for resume assessment. In *Proceedings of the 30th ACM International Conference on Multimedia*, MM '22, page 1612–1620, New York, NY, USA, 2022. Association for Computing Machinery.

[79] Shanliang Yao, Runwei Guan, Zhaodong Wu, Yi Ni, Zile Huang, Ryan Wen Liu, Yong Yue, Weiping Ding, Eng Gee Lim, Hyungjoon Seo, et al. Waterscenes: A multi-task 4d radar-camera fusion dataset and benchmarks for autonomous driving on water surfaces. *IEEE Transactions on Intelligent Transportation Systems*, 2024.

[80] Wang Yinglong and He Bin. Casdyf-net: Image dehazing via cascaded dynamic filters. *arXiv preprint arXiv:2409.08510*, 2024.

[81] Qihang Yu, Ju He, Xueqing Deng, Xiaohui Shen, and Liang-Chieh Chen. Convolutions die hard: Open-vocabulary segmentation with single frozen convolutional clip. *Advances in Neural Information Processing Systems*, 36:32215–32234, 2023.

[82] Jieyu Yuan, Zhanchuan Cai, and Wei Cao. Tebcf: Real-world underwater image texture enhancement model based on blurriness and color fusion. *IEEE Transactions on Geoscience and Remote Sensing*, 60:1–15, 2021.

[83] Hao Zhang, Feng Li, Shilong Liu, Lei Zhang, Hang Su, Jun Zhu, Lionel M Ni, and Heung-Yeung Shum. Dino: Detr with improved denoising anchor boxes for end-to-end object detection. *arXiv preprint arXiv:2203.03605*, 2022.

[84] Lojze Žust and Matej Kristan. Learning maritime obstacle detection from weak annotations by scaffolding. In *Proceedings of the IEEE/CVF Winter Conference on Applications of Computer Vision*, pages 955–964, 2022.

[85] Lojze Žust and Matej Kristan. PanSR: An object-centric mask transformer for panoptic segmentation. *arXiv preprint arXiv:2412.10589*, 2024.

[86] Lojze Žust, Janez Perš, and Matej Kristan. LaRS: A diverse panoptic maritime obstacle detection dataset and benchmark. In *International Conference on Computer Vision (ICCV)*, 2023.